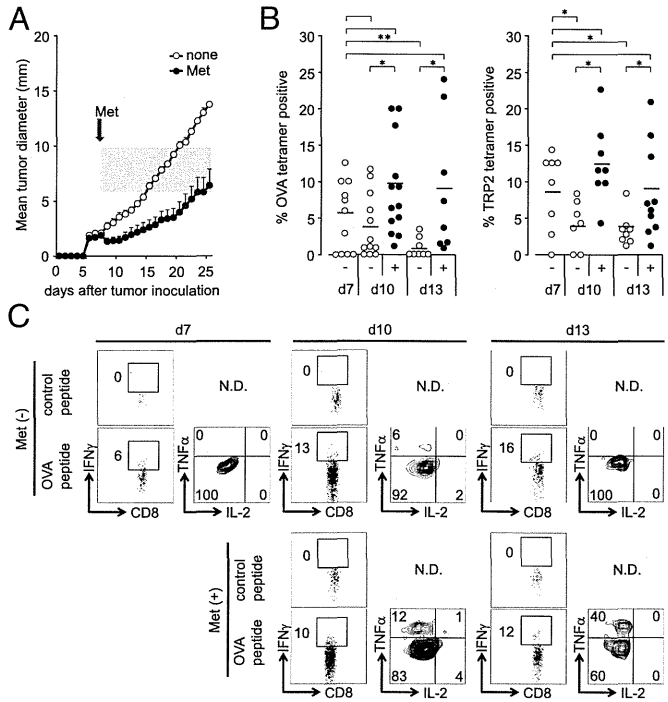

Fig. 2. Metformin improves the multifunctionality of antigen-specific CD8$^+$ TILs in vivo. (*A*) Mice inoculated with 2×10^5 MO5 cells were treated with or without metformin from day 7, as indicated by the shadowed rectangle, and tumor growth was monitored. The results are representative of two independent experiments. $n = 5$ per group. (*B*) On days 7, 10, and 13, TILs were recovered from tumor masses and examined for K^b-$OVA_{257-264}$ and K^b-$TRP2_{180-188}$ tetramer binding ($n = 7$–13). (*C*) TILs recovered on days 7, 10, and 13 from five mice per group [with (+) or without (–) metformin] were pooled and stimulated with DC2.4 cells that had been prepulsed with $OVA_{257-265}$ peptide (10^{-6} M) for 8 h; TIL cytokine-producing ability was later examined.

Annexin V (Fig. 1*F* and Fig. S3*A*), and that metformin suppressed apoptosis induction in all subsets, including PD-1$^-$Tim-3$^+$CD8$^+$TILs (Fig. S3 *B*–*E*). Of note, the physiologically essential apoptotic process of CD4$^+$CD8$^+$ thymocytes, which depends on a mitochondrial pathway (32), was not down-regulated by metformin (Fig. S4), suggesting that an apoptotic mechanism unique to the tumor microenvironment is metformin-sensitive.

We next examined the metformin effects in another tumor system. MO5 is a subclone of B16 melanoma cells expressing ovalbumin (OVA) (33). Metformin administration induced significant antitumor activity (Fig. 2*A*). OVA- and TRP2-specific CD8$^+$ TILs were identified by specific tetramers. Both TIL populations in untreated mice decreased gradually from day 7–13; in contrast, metformin administration maintained or increased these populations (Fig. 2*B*). CD8$^+$ TILs again underwent apoptosis, which was suppressed by metformin administration (Fig. S5 *A* and *B*). The Annexin V-positive populations among OVA tetramer-positive and -negative (includes TRP-2–positive population) CD8$^+$ TILs were near 80% at day 10; however, metformin suppressed this rate to <20–40% (Fig. S5 *C* and *D*). These results are consistent with those observed in the RLmale1 model. Next, to examine the functional state of antigen-specific TILs, magnet-purified CD8$^+$ TILs isolated from tumor tissues were incubated with DC-like DC2.4 cells that had been pulsed with an epitope peptide ($OVA_{257-264}$); TILs were later examined for their cytokine production capacity. Only IFNγ-producing cells or very small populations producing both IFNγ and TNFα or IL-2 could be identified in untreated mice, whereas a marked increase in the population producing both IFNγ and TNFα was observed with metformin (Fig. 2*C*).

Influence of Metformin on the TCM/TEM Ratio of CD8$^+$TILs. CD8$^+$ TILs in the context of memory T cells are poorly understood. Elegant studies with an acute viral infection model have proposed classification of memory T cells into central memory (TCM; CD44$^+$, CD62L^{high}) and effector memory (TEM; CD44$^+$, CD62L^{low}) (34, 35). TCM were shown to mediate viral-specific recall responses. Based on this model, we investigated TCM and TEM CD8$^+$ TILs. Without metformin, the staining of CD8$^+$ TILs from an RLmale1 tumor using antibodies against CD62L and CD44 revealed that proportions of TCM and TEM were nearly equal on day 7 and 10 but shifted to TCM dominance on day 13. In contrast, metformin maintained TEM dominance from day 10 to day 13 (Fig. 3*A*). Further dissection of the TIL compartment based on CD62L and KLRG1 expression revealed that short-lived effector T cells (TE; CD62L^{low}KLRG1^{high}) were visible on day 7 but gradually decreased by day 13. In contrast, metformin yielded increases in both TEM and TE populations on day 13 (Fig. 3*B*), coinciding with tumor regression (Fig. 1*A*). In the MO5 model, metformin again caused TEM dominant over TCM (Fig. 3 *C* and *D*). At this stage, we concluded that TEM and/or TE are more responsible than TCM for tumor rejection.

Metformin Induced Multifunctional CD8$^+$ TEM Expressing the Exhaustion Marker Tim-3. We next investigated the capacity for triple cytokine (IL-2, TNFα, IFNγ) production or the multifunctionality of CD8$^+$ TILs in the context of TCM/TEM classification. CD8$^+$ TILs recovered from RLmale1 tumor masses were stimulated with PMA/ionomycin for 6 h in vitro and monitored for cytokine production. Without metformin, the cytokine-producing cells on day 10 were mainly identified as TCM (Fig. 4*A*). In contrast, with metformin, triple cytokine-producing cells appeared in correlation with the increased population of TEM (Fig. 4*A*). The populations with various cytokine producing patterns in the presence and absence of metformin are summarized in Fig. 4*B*. Metformin markedly changed the multifunctionality of CD8$^+$ TILs. Taking these results together, we concluded that metformin-induced TEM capable of producing

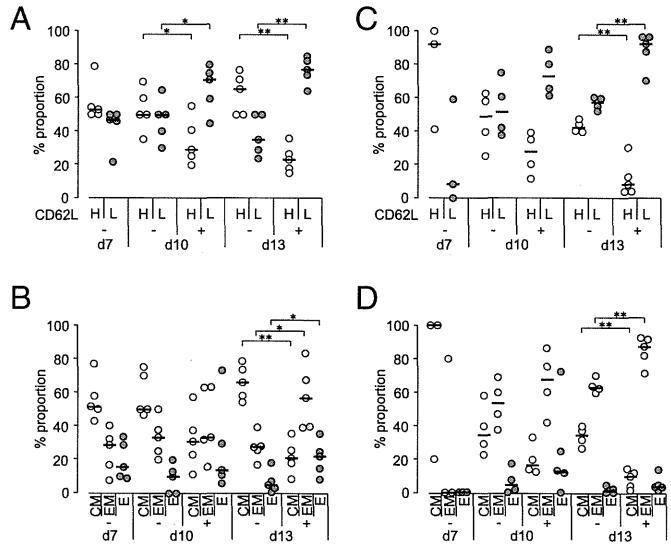

Fig. 3. Influence of metformin on the TCM/TEM ratio of CD8$^+$ TILs. TILs were isolated on days 7, 10, and 13 from mice inoculated with RLmale1 (*A* and *B*, $n = 5$) or MO5 (*C* and *D*, $n = 3$–5) with (+) or without (–) metformin, and analyzed for CD8 and memory markers including CD44, CD62L, KLRG1. The proportion (%) of CD62L^{high} (H) and CD62L^{low} (L) among CD44$^+$ cells in RLmale1 and MO5 models are shown in *A* and *C*, respectively. The proportion (%) of CD62L^{high}, KLRG1^{low} (central memory; CM) and CD62L^{low}, KLRG1 ^{low} (effector memory; EM) and CD62L^{low}, KLRG1 ^{high} (effector; E) in RLmale1 and MO5 are shown in *B* and *D*, respectively. $^*P < 0.05$, $^{**}P < 0.01$.

multiple (triple and double) cytokines are most important for tumor rejection. We next classified $CD8^+$ TILs on the basis of their expression of PD-1 and Tim-3, followed by intracellular cytokine staining. We found that $CD8^+$ TILs with triple cytokine-producing abilities belonged exclusively to the PD-1^-Tim-3^+ subset, which was the supposedly exhausted population in the RLmale1 tumor model (Fig. S6). We further confirmed this notion using adoptive transfer experiments. MO5-inoculated mice were adoptively transferred with OT-I $CD8^+$ T cells. The transferred T cells had been previously shown to undergo vigorous division and were thus cross-primed in vivo via the adjuvant-free administration of a fusion protein comprising OVA and *Mycobacterium* heat shock protein 70 (OVA-mHSP70) as a vaccine (36, 37). OVA-mHSP70 injection significantly enhanced the migration of the transferred CD45.1^+OT-I $CD8^+$ T cells into the tumor tissues; however, the cytokine-producing abilities of these cells were poor (Fig. 5*A*). In contrast, injection of the fusion protein together with oral metformin administration apparently improved the multifunctionality of the migrated T cells, which were classified as the Tim-3^+ population (Fig. 5*A*).

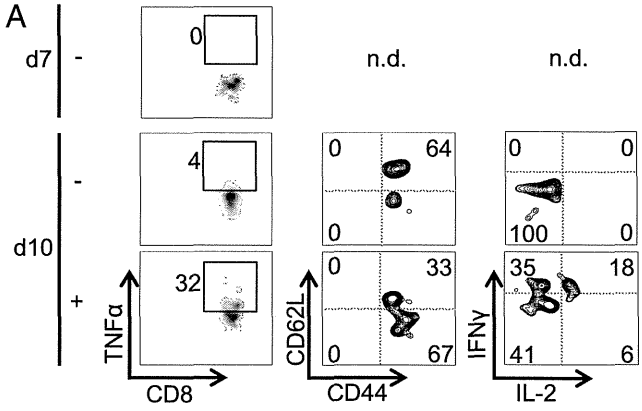

B

cytokine	Met (-)	Met (+)
IL-2^+TNFα^+IFNγ^+	-	4.6-7.2% (169-264)
IL-2^+TNFα^+IFNγ^-	-	1.3-1.9% (48-69)
IL-2^+TNFα^-IFNγ^+	-	5.3-7.2% (194-264)
IL-2^-TNFα^+IFNγ^+	-	7.2-11.2% (264-411)
IL-2^+TNFα^-IFNγ^-	2.0% (15)	1.7% (62)
IL-2^-TNFα^+IFNγ^-	4.0% (30)	13.1% (480)
IL-2^-TNFα^-IFNγ^+	9.0% (67)	36.0% (1320)

Fig. 4. Metformin-induced $CD8^+$TILs with multifunctionality are TEM rather than TCM. (*A*) TILs were isolated on the indicated days from five mice per group inoculated with 2×10^5 RLmale1. Met treatment was started (+) or not (–) from day 7. TILs were then pooled on indicated days and stimulated with PMA/ionomycin for 6 h, stained for surface molecules including CD8, CD44, CD62L, followed by intracellular staining for IL-2, TNFα, and IFNγ. $CD8^+$TILs producing TNFα were further analyzed for expression of CD62L and CD44 to identify TCM and TEM. Also, to investigate multifunctionality, cytokine-producing $CD8^+$TILs were further examined for production of IFNγ and IL-2. (*B*) Summary of the populations of cytokine producing $CD8^+$TILs on day 10 is shown. Gated populations for $CD8^+$IFNγ^+, $CD8^+$TNFα^+, or $CD8^+$IL-2^+ were further analyzed for their production of TNFα and IL-2, IFNγ and IL-2, or IFNγ and TNFα. The gating strategy gives rise to some ranges for % populations of double and triple cytokine producing TILs. The numbers within parenthesis indicate numbers of corresponding $CD8^+$TILs per tumor volume (mm^3).

Metformin-Treated Antigen-Specific Naïve CD8 T Cells Migrate into Tumors and Exert Antitumor Immunity Following Adoptive Transfer. It is unknown whether plasma metformin concentrations as low as 10 μM (1.6 μg/mL) would directly influence the fate of T cells. To address this important question, we incubated $CD8^+$ T cells isolated from naïve OT-I mice with 10 μM metformin for 6 h in the presence or absence of different doses of the AMPK inhibitor compound C (38) as indicated (Fig. 5*B*). After extensive washing, the cells were transferred into MO5-bearing mice. Two days later, splenic T cells and TILs were recovered and investigated for the presence and multifunctionality of donor-derived $CD8^+$ T cells. Metformin-treated $CD8^+$ TILs comprised up to 9.9% of all $CD8^+$ T cells and were identified as triple cytokine-producing cells (Fig. 5*B*). However, compound C treatment abrogated the migration, although donor $CD8^+$ T cells were present in the spleens of all groups (Fig. 5*B*). Accordingly, tumor growth inhibition was apparent in the metformin-treated group, although this effect was blocked by compound C (Fig. 5*C*). The weak but significant metformin-mediated increase in the phosphorylation of AMPK and its downstream target acetyl-CoA carboxylase (ACC) and the abrogation of this effect by compound C were observed by Western blot analysis (Fig. 5*D*). The results led us to conclude that the direct action of metformin on $CD8^+$ T cells, at least partly, reduced their exhaustion within the tumor microenvironment in a manner sensitive to the AMPK inhibitor compound C.

AMPK Phosphorylation, Enhanced Bat3 Expression, and Caspase-3 Inhibition Mediated by Metformin. Finally, we examined the expression of $CD8^+$ TIL molecules that may possibly be influenced by metformin administration. After $CD8^+$ TIL purification on day 10, cell lysates were immediately prepared for candidate molecule detection via Western blot analysis and for caspase-3 activity measurement using a fluorescent substrate. The levels of phosphorylated AMPKα and β were increased; a twofold increase in Bat3 expression was also observed, whereas Bcl2 and Bax expression were unaltered (Fig. S7*A*). As expected, caspase-3 activity was prominent without metformin but was completely abrogated in $CD8^+$ TILs from metformin-treated mice (Fig. S7*B*), which offers a plausible explanation for apoptosis inhibition. To further examine the apoptotic cell populations, we evaluated the expression of active caspase-3 in TCM, TEM, and TE. Without metformin, TCM, TEM, and TE all expressed active caspase-3 whereas with metformin, primarily TCM expressed this activated enzyme (Fig. S7*C*). These results may explain the dominance of TCM over TEM in the absence of metformin and the dominance of TEM and TE in the presence of metformin. pS6, a downstream target of mTOR, was positive in TCM, TEM, and TE without metformin but negative with metformin (Fig. S7*D*), indicating that metformin inhibits mTOR, possibly via AMPK activation.

Discussion

In this report, we showed that established solid tumors are regressed by oral administration of metformin, and that $CD8^+$T cells mediate this effect. The number of FoxP3 expressing $CD4^+$ regulatory T cells (Treg) has been implicated as a critical component in suppressing tumor immunity (39). However, their numbers were not decreased, rather, transiently increased by metformin administration in RLmale 1 tumor model (Fig. S8). Upon tumor rejection, the treated mice became resistant to rechallenge with the same tumor, providing proof of memory T-cell generation. Because no protective effect was observed in SCID mice, the direct killing of tumor cells by metformin is negligible. It was also confirmed by immunohistochemistry (IHC) of tumors. Tumors of mice treated with metformin showed decreased expression of Ki67 as a proliferation marker, accordingly, increased expression of active caspase 3 as an

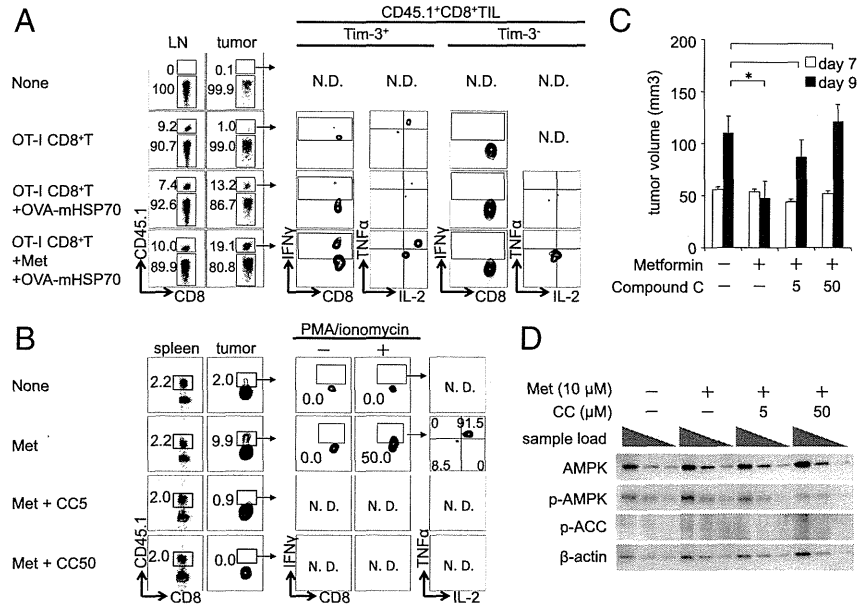

Fig. 5. Metformin use for combination with vaccine or cell therapy using CD8T cells. (*A*) Combined use of cancer vaccines and metformin improves $CD8^+$ TIL multifunctionality. B6 mice (CD45.2) inoculated with 3×10^5 MO5 cells were adoptively transferred or not with 2×10^6 CD45.1/OT-I $CD8^+$ T cells on day 7 (n = 5). Simultaneously, 10 μg of the OVA-mHSP70 fusion protein were i.v. injected along with or without the oral administration of 5 mg/mL metformin as indicated. Three days later, the right inguinal lymph nodes (LNs) and tumor masses were removed, prepared as single-cell suspensions. The cells were stimulated with PMA/ionomycin, followed by labeling with antibodies and were subjected to flow cytometric analysis. (*B*) Metformin-treated antigen-specific naïve CD8 T cells acquire multifunctionality within the tumor. B6 mice (CD45.2) inoculated with MO5 cells were adoptively transferred or not with 3×10^6 CD45.1/OT-I CD8 T cells on day 7 (n = 5). The cells to be transferred were isolated from CD45.1 OT-1 mice and precultured with 10 μM metformin with or without compound C (5, 50 μM) for 6 h before transfer. Two days later, the spleen and tumor tissues were removed and prepared as single-cell suspensions. The cells were then investigated for migration and multifunctionality. (*C*) The mean tumor diameters were measured on days 7 and 9 after MO5 inoculation and were plotted with SE. (*D*) The Western blot detection of AMPK, p-AMPK, and p-ACC in $CD8^+$ T cells treated with metformin in vitro. Anti-actin was used as a loading control. OT-1 CD8 T cells treated in *A* were lysed, titrated 1-, 1/2-, and 1/4-fold, and subjected to the assay.

apoptosis marker; however, the effect was abrogated by CD8 T-cell depletion (Fig. S9). Our used model systems comprised highly immunogenic tumors, and it is unclear whether metformin would have the same effect on less immunogenic tumors. Demonstration of a similar effect in an autochthonous tumor model would be required in the future. Nonetheless, metformin countered apoptotic induction and reduced cytokine production in $CD8^+$ TILs and thus blocked immune exhaustion within the tumor tissues we tested. The adoptive transfer experiment shown in Fig. 5 further demonstrated that the direct effect of metformin on $CD8^+$ T cells, even at a physiologically relevant low concentration, markedly altered the cells' multifunctionality following migration into the tumor. Experiments with a genetic approach will be required to fully demonstrate whether this effect is mediated via AMPK activation in $CD8^+$ T cells, because compound C is not highly specific for AMPK.

Dissection of TILs from the point of view of memory T cells in the context of multifunctionality provides mechanistic insight into metformin-induced antitumor immunity. Memory T cells have been classified as TCM, migrating between lymphoid organs, and TEM, circulating principally in the blood, spleen and peripheral tissues (34, 35, 40). In acute virus infection models, as the virus is cleared, the population of TCM progressively increase, whereas the total numbers of TEM rapidly decrease (41). The naturally occurring proportional shift from TEM to TCM, however, was not associated with metformin-induced rejection in the tumor models. For example, in the absence of metformin in the RLmale1 model, the TCM population gradually increased to exceed the TEM population by day 13 (Fig. 3 *A* and *B*); however, this proportional shift to TCM was associated with progressive tumor growth rather than tumor regression. Metformin possibly affects the TCM/TEM ratio by regulating TEM apoptosis (Fig. S7*C*). The consequent decreased TCM/TEM ratio was apparently associated with antitumor activity in both the RLmale1 and MO5 models.

Analysis of the cytokine-producing capacities of $CD8^+$ TILs also revealed the importance of TEM over TCM. A significant proportion of the $CD8^+$ TIL population was maintained by metformin and produced IL-2, TNFα, and IFNγ. These triple cytokine-producing $CD8^+$ TILs were exclusively of the $PD1^-Tim3^+$ phenotype (Fig. S6), which is committed to a TEM rather than a TCM fate (Fig. 4). Moreover, although therapeutic vaccination with OVA-mHSP70 stimulated the migration of adoptively transferred OT-I $CD8^+$ T cells into tumor tissues, these TILs lost multifunctionality (Fig. 5*A*). Possibly, the cells were exhausted from the tumor microenvironment. Coadministration of metformin, however, led to the activation of the migrated $Tim\text{-}3^+$ OT-I $CD8^+$ T cells and the production of multiple cytokines (Fig. 5*A*). Therefore, combined use of metformin and cancer vaccines may improve the efficacy of the vaccine. These findings provide novel insights into anticancer immunity. It is possible that tumor persistence stimulates the development of $CD8^+$ TILs into TCM cells, which will immediately become useless against tumor growth because of immune exhaustion, and that metformin counters this situation, leading to the conversion of TCM to activated-state TEM that are fully active against tumors, despite exhibiting the surface phenotype of an exhausted cell (e.g., Tim-3 expression).

A previous report found that metformin treatment following vaccination with attenuated *Listeria monocytogenes* expressing OVA (LmOVA) protected mice from challenge by tumor cells expressing OVA (42). This effect was caused by metformin-induced expansion of memory T cells after vaccination. As the tumor challenge occurred after metformin withdrawal, it is a matter of a prophylactic vaccination effect, which is different from the effects on immune exhaustion states in the tumor microenvironment.

mTOR inhibition is among the downstream consequences of AMPK signaling, which is activated by metformin. Therefore, rapamycin, an inhibitor of mTORC1, may share mechanistic effects with metformin. Rapamycin has been shown to promote the generation of memory T cells (42–44) particularly in viral infection models. A common feature in the results was the increased population of TCM over TEM consequent to rapamycin treatment (45). In our tumor models, however, metformin treatment preferentially increased the TEM population. It remains possible that additional pharmacological effects are involved in response to metformin versus rapamycin treatment. Further experiments will be required to elucidate cellular and molecular mechanism underlying metformin-induced reversion of exhausted $CD8^+$TILs.

Materials and Methods

Mice. BALB/c and C57BL/6 (B6) mice were purchased from CLEA Japan and SLC. Breeding pairs of CB-17 SCID mice were provided by K. Kuribayashi, Mie University School of Medicine, Mie, Japan.

Tumor Cell Lines. BALB/c radiation leukemia RLmale1, B6 OVA-gene introduced B16 melanoma MO5, B6 nonsmall cell lung carcinoma 3LL, BALB/c intestinal carcinoma Colon 26, BALB/c renal cell carcinoma Renca, and BALB/c breast cancer cell 4T1 were used for the tumor assay. 3LL, Colon 26, Renca, and 4T1 were kindly provided by H. Yagita, Juntendo University School of Medicine, Tokyo, Japan.

Tumor Growth Assay. Mice were intradermally inoculated with 2×10^5 tumor cells (in 0.2 mL) on the right back with a 27-gauge needle. Before inoculation of tumor cells, the hair was cut with clippers. Mice were orally administrated metformin hydrochloride (Wako) (5 mg/mL) or as indicated dissolved the drinking water. The diameter of the tumors was measured with Vernier calipers twice at right angles to calculate the mean diameter.

ACKNOWLEDGMENTS. We thank Ms. Yamashita for technical assistance and Dr. Toshifumi Matsuyama for critical reading of the manuscript and discussion about this work. This work was supported by grants from the Projects for Development of Innovative Research on Cancer Therapeutics by the Ministry of Education, Culture, Sports, Science, and Technology of Japan; Health and Labor Sciences Research Grants; Research on Applying Health Technology in Japan; The Naito Foundation; Takeda Science Foundation; and The Secom Science and Technology Foundation.

1. Wherry EJ (2011) T cell exhaustion. *Nat Immunol* 12(6):492–499.
2. Dong H, et al. (2002) Tumor-associated B7-H1 promotes T-cell apoptosis: A potential mechanism of immune evasion. *Nat Med* 8(8):793–800.
3. Blank C, et al. (2004) PD-L1/B7H-1 inhibits the effector phase of tumor rejection by T cell receptor (TCR) transgenic $CD8^+$ T cells. *Cancer Res* 64(3):1140–1145.
4. Iwai Y, et al. (2002) Involvement of PD-L1 on tumor cells in the escape from host immune system and tumor immunotherapy by PD-L1 blockade. *Proc Natl Acad Sci USA* 99(19):12293–12297.
5. Zhu C, et al. (2005) The Tim-3 ligand galectin-9 negatively regulates T helper type 1 immunity. *Nat Immunol* 6(12):1245–1252.
6. Ngiow SF, et al. (2011) Anti-TIM3 antibody promotes T cell IFN-γ-mediated antitumor immunity and suppresses established tumors. *Cancer Res* 71(10):3540–3551.
7. Sakuishi K, et al. (2010) Targeting Tim-3 and PD-1 pathways to reverse T cell exhaustion and restore anti-tumor immunity. *J Exp Med* 207(10):2187–2194.
8. Sakuishi K, Jayaraman P, Behar SM, Anderson AC, Kuchroo VK (2011) Emerging Tim-3 functions in antimicrobial and tumor immunity. *Trends Immunol* 32(8):345–349.
9. Pardoll DM (2012) The blockade of immune checkpoints in cancer immunotherapy. *Nat Rev Cancer* 12(4):252–264.
10. Bailey CJ (1992) Biguanides and NIDDM. *Diabetes Care* 15(6):755–772.
11. Bailey CJ, Turner RC (1996) Metformin. *N Engl J Med* 334(9):574–579.
12. UK Prospective Diabetes Study (UKPDS) Group (1998) Effect of intensive blood-glucose control with metformin on complications in overweight patients with type 2 diabetes (UKPDS 34). *Lancet* 352(9131):854–865.
13. McFarland MS, Cripps R (2010) Diabetes mellitus and increased risk of cancer: focus on metformin and the insulin analogs. *Pharmacotherapy* 30(11):1159–1178.
14. Colhoun HM; SDRN Epidemiology Group (2009) Use of insulin glargine and cancer incidence in Scotland: a study from the Scottish Diabetes Research Network Epidemiology Group. *Diabetologia* 52(9):1755–1765.
15. Currie CJ, Poole CD, Gale EA (2009) The influence of glucose-lowering therapies on cancer risk in type 2 diabetes. *Diabetologia* 52(9):1766–1777.
16. Hemkens LG, et al. (2009) Risk of malignancies in patients with diabetes treated with human insulin or insulin analogues: A cohort study. *Diabetologia* 52(9):1732–1744.
17. Jonasson JM, et al. (2009) Insulin glargine use and short-term incidence of malignancies-a population-based follow-up study in Sweden. *Diabetologia* 52(9):1745–1754.
18. Bodmer M, Meier C, Krähenbühl S, Jick SS, Meier CR (2010) Long-term metformin use is associated with decreased risk of breast cancer. *Diabetes Care* 33(6):1304–1308.
19. Evans JM, Donnelly LA, Emslie-Smith AM, Alessi DR, Morris AD (2005) Metformin and reduced risk of cancer in diabetic patients. *BMJ* 330(7503):1304–1305.
20. Bowker SL, Majumdar SR, Veugelers P, Johnson JA (2006) Increased cancer-related mortality for patients with type 2 diabetes who use sulfonylureas or insulin. *Diabetes Care* 29(2):254–258.
21. Libby G, et al. (2009) New users of metformin are at low risk of incident cancer: a cohort study among people with type 2 diabetes. *Diabetes Care* 32(9):1620–1625.
22. Decensi A, et al. (2010) Metformin and cancer risk in diabetic patients: A systematic review and meta-analysis. *Cancer Prev Res (Phila)* 3(11):1451–1461.
23. Noto H, Goto A, Tsujimoto T, Noda M (2012) Cancer risk in diabetic patients treated with metformin: a systematic review and meta-analysis. *PLoS ONE* 7(3):e33411.
24. Anisimov VN, et al. (2005) Effect of metformin on life span and on the development of spontaneous mammary tumors in HER-2/neu transgenic mice. *Exp Gerontol* 40(8-9):685–693.
25. Rocha GZ, et al. (2011) Metformin amplifies chemotherapy-induced AMPK activation and antitumoral growth. *Clin Cancer Res* 17(12):3993–4005.
26. Hirsch HA, Iliopoulos D, Tsichlis PN, Struhl K (2009) Metformin selectively targets cancer stem cells, and acts together with chemotherapy to block tumor growth and prolong remission. *Cancer Res* 69(19):7507–7511.
27. Sato A, et al. (2012) Glioma-initiating cell elimination by metformin activation of FOXO3 via AMPK. *Stem Cells Transl Med* 1(11):811–824.
28. Song CW, et al. (2012) Metformin kills and radiosensitizes cancer cells and preferentially kills cancer stem cells. *Sci Rep* 2:362.
29. Shank JJ, et al. (2012) Metformin targets ovarian cancer stem cells in vitro and in vivo. *Gynecol Oncol* 127(2):390–397.
30. Uenaka A, et al. (1994) Identification of a unique antigen peptide pRL1 on BALB/c RL male 1 leukemia recognized by cytotoxic T lymphocytes and its relation to the Akt oncogene. *J Exp Med* 180(5):1599–1607.
31. Memmott RM, et al. (2010) Metformin prevents tobacco carcinogen—induced lung tumorigenesis. *Cancer Prev Res (Phila)* 3(9):1066–1076.
32. Hogquist KA, Baldwin TA, Jameson SC (2005) Central tolerance: Learning self-control in the thymus. *Nat Rev Immunol* 5(10):772–782.
33. Ryu MS, et al. (2014) Accumulation of cytolytic $CD8^+$ T cells in B16-melanoma and proliferation of mature T cells in TIS21-knockout mice after T cell receptor stimulation. *Exp Cell Res* 327(2):209–221.
34. Sallusto F, Lenig D, Förster R, Lipp M, Lanzavecchia A (1999) Two subsets of memory T lymphocytes with distinct homing potentials and effector functions. *Nature* 401(6754):708–712.
35. Masopust D, Vezys V, Marzo AL, Lefrançois L (2001) Preferential localization of effector memory cells in nonlymphoid tissue. *Science* 291(5512):2413–2417.
36. Suzue K, Zhou X, Eisen HN, Young RA (1997) Heat shock fusion proteins as vehicles for antigen delivery into the major histocompatibility complex class I presentation pathway. *Proc Natl Acad Sci USA* 94(24):13146–13151.
37. Mizukami S, Kajiwara C, Tanaka M, Kaisho T, Udono H (2012) Differential MyD88/IRAK4 requirements for cross-priming and tumor rejection induced by heat shock protein 70-model antigen fusion protein. *Cancer Sci* 103(5):851–859.
38. Zhou G, et al. (2001) Role of AMP-activated protein kinase in mechanism of metformin action. *J Clin Invest* 108(8):1167–1174.
39. Onizuka S, et al. (1999) Tumor rejection by in vivo administration of anti-CD25 (interleukin-2 receptor α) monoclonal antibody. *Cancer Res* 59(13):3128–3133.
40. Reinhardt RL, Khoruts A, Merica R, Zell T, Jenkins MK (2001) Visualizing the generation of memory CD4 T cells in the whole body. *Nature* 410(6824):101–105.
41. Kedzierska K, Valkenburg SA, Doherty PC, Davenport MP, Venturi V (2012) Use it or lose it: establishment and persistence of T cell memory. *Front Immunol* 3:357.
42. Pearce EL, et al. (2009) Enhancing CD8 T-cell memory by modulating fatty acid metabolism. *Nature* 460(7251):103–107.
43. Araki K, et al. (2009) mTOR regulates memory CD8 T-cell differentiation. *Nature* 460(7251):108–112.
44. Rao RR, Li Q, Odunsi K, Shrikant PA (2010) The mTOR kinase determines effector versus memory $CD8^+$ T cell fate by regulating the expression of transcription factors T-bet and Eomesodermin. *Immunity* 32(1):67–78.
45. Araki K, Youngblood B, Ahmed R (2010) The role of mTOR in memory CD8 T-cell differentiation. *Immunol Rev* 235(1):234–243.

Published OnlineFirst August 15, 2014; DOI: 10.1158/2326-6066.CIR-14-0098

Research Article

Cancer Immunology Research

Cytotoxic T Lymphocytes Block Tumor Growth Both by Lytic Activity and IFNγ-Dependent Cell-Cycle Arrest

Hirokazu Matsushita[1], Akihiro Hosoi[1,2], Satoshi Ueha[3], Jun Abe[3], Nao Fujieda[1,2], Michio Tomura[4], Ryuji Maekawa[2], Kouji Matsushima[3], Osamu Ohara[5], and Kazuhiro Kakimi[1]

Abstract

To understand global effector mechanisms of CTL therapy, we performed microarray gene expression analysis in a murine model using pmel-1 T-cell receptor (TCR) transgenic T cells as effectors and B16 melanoma cells as targets. In addition to upregulation of genes related to antigen presentation and the MHC class I pathway, and cytotoxic effector molecules, cell-cycle–promoting genes were downregulated in the tumor on days 3 and 5 after CTL transfer. To investigate the impact of CTL therapy on the cell cycle of tumor cells *in situ*, we generated B16 cells expressing a fluorescent ubiquitination-based cell-cycle indicator (B16-fucci) and performed CTL therapy in mice bearing B16-fucci tumors. Three days after CTL transfer, we observed diffuse infiltration of CTLs into the tumor with a large number of tumor cells arrested at the G_1 phase of the cell cycle, and the presence of spotty apoptotic or necrotic areas. Thus, tumor growth suppression was largely dependent on G_1 cell-cycle arrest rather than killing by CTLs. Neutralizing antibody to IFNγ prevented both tumor growth inhibition and G_1 arrest. The mechanism of G_1 arrest involved the downregulation of S-phase kinase-associated protein 2 (Skp2) and the accumulation of its target cyclin-dependent kinase inhibitor p27 in the B16-fucci tumor cells. Because tumor-infiltrating CTLs are far fewer in number than the tumor cells, we propose that CTLs predominantly regulate tumor growth via IFNγ-mediated profound cytostatic effects rather than via cytotoxicity. This dominance of G_1 arrest over other mechanisms may be widespread but not universal because IFNγ sensitivity varied among tumors. *Cancer Immunol Res; 3(1); 26–36. ©2014 AACR.*

See related commentary by Riddell, p. 23

Introduction

Adoptive T-cell immunotherapy (ACT) using autologous tumor-infiltrating lymphocytes (TIL) can be highly effective for treating melanoma (1). The recent development of genetically engineered T cells stably expressing exogenous T-cell receptors (TCR) or chimeric antigen receptors (CAR) specific for tumor-associated antigens offers the possibility of testing the efficacy of ACT against a wide range of cancer types in addition to melanoma (2, 3). Many clinical trials have now been conducted using genetically engineered T cells specific for tumor antigens as well as TILs, and some objective responses have been achieved (4, 5). It is clear from mouse models that adoptively transferred antigen-specific T cells are capable of eradicating established cancer (6–8), and the ability of CTLs to directly kill tumor and/or stromal cells is thought to be important for tumor elimination (9–11). Nonetheless, cytokines such as IFNγ and TNFα produced by T cells are also likely to contribute to the prevention of tumor growth by ACT via mechanisms other than cell lysis (12–14).

IFNγ is a critical cytokine for antitumor immunity under natural and therapeutic conditions (15, 16). It enhances tumor immunogenicity by upregulating components of the MHC antigen processing and presentation pathway. It also induces the expression of chemokines, including the angiostatic chemokines CXCL9 (MIG), CXCL10 (IP-10), and CXCL11 (I-TAC), that block neovascularization in the tumor and recruit effector immune cells (17–19). Furthermore, IFNγ has been reported to exert antiproliferative effects on the developing tumor (20, 21), and it triggers apoptosis of tumor cells by inducing proapoptotic molecules (22, 23).

To understand the global antitumor effect mediated by ACT, we used the B16 melanoma pmel-1 TCR-transgenic T-cell model to perform a gene expression analysis of ACT-treated tumors. On the basis of these results, we focused on genes controlling the cell cycle and arresting growth of B16 tumor cells in this model. We examined the effects on tumor cells of the IFNγ produced by the CTLs *in situ* using cell-cycle status indicators and investigated the mechanism of cell-cycle arrest. Furthermore, we demonstrate the importance of cell-cycle arrest induced by CTL-derived IFNγ in the regulation of tumor growth.

[1]Department of Immunotherapeutics, The University of Tokyo Hospital, Tokyo, Japan. [2]Medinet Co Ltd., Yokohama, Japan. [3]Department of Molecular Preventive Medicine, Graduate School of Medicine, The University of Tokyo, Tokyo, Japan. [4]Center for Innovation in Immunoregulative Technology and Therapeutics, Kyoto University Graduate School of Medicine, Kyoto, Japan. [5]Department of Human Genome Research, Kazusa DNA Research Institute, Chiba, Japan.

Note: Supplementary data for this article are available at Cancer Immunology Research Online (http://cancerimmunolres.aacrjournals.org/).

Corresponding Author: Kazuhiro Kakimi, Department of Immunotherapeutics, The University of Tokyo Hospital, 7-3-1 Hongo, Bunkyo-Ku, Tokyo 113-8655, Japan. Phone: 81-3-5805-3161; Fax: 81-3-5805-3164; E-mail: kakimi@m.u-tokyo.ac.jp

doi: 10.1158/2326-6066.CIR-14-0098

Published OnlineFirst August 15, 2014; DOI: 10.1158/2326-6066.CIR-14-0098

Materials and Methods

Mice, tumor cells, and peptides

Six-week-old male C57BL/6 mice were purchased from Japan SLC. Mice transgenic for the pmel-1-TCR, which recognizes the H-2D^b–restricted epitope EGSRNQDWL from gp100 (gp100$_{25-33}$), were obtained from The Jackson Laboratory. All mice were housed in a pathogen-free environment, and all animal procedures were conducted in accordance with institutional guidelines. All animal experiments were approved by the University of Tokyo Ethics Committee for Animal Experiments (10-P-127). The H-2D^b–restricted peptide human gp100 (hgp100$_{25-33}$, KVPRNQDWL) was purchased from GenScript Japan at a purity of >90%, with free amino and carboxyl terminals. B16F10, FBL3, and 3LL cell lines were maintained in culture medium consisting of DMEM with 10% FCS, 100 U/mL penicillin, and 100 μg/mL streptomycin. EL4, P815, and CT26 were cultured in RPMI-1640 medium supplemented with 10% FCS, 100 U/mL penicillin, and 100 μg/mL streptomycin. All cell lines were tested for Mycoplasma by the MycoAlert Mycoplasma Detection kit (Lonza). Cellular morphology and growth curve *in vitro* were checked in all cell lines. B16F10 and B16-fucci cells were authenticated by transplantation for assessing growth ability *in vivo*.

Dendritic cell preparation and CTL stimulation

Dendritic cells (DC) were obtained by 8-day culture of C57BL/6-derived bone marrow cells with granulocyte-macrophage colony-stimulating factor (GM-CSF), as described previously (24). Briefly, bone marrow cells obtained from tibias and femurs of C57BL/6 mice were cultured in RPMI-1640 medium supplemented with 10% FCS, 10 mmol/L HEPES, 5×10^{-5} mol/L 2-mercaptoethanol, 1×10^{-3} mol/L sodium pyruvate, 1% nonessential amino acids, 100 U/mL penicillin, 100 μg/mL streptomycin, and 20 ng/mL GM-CSF (PeproTech) for 8 days. On days 3 and 6, half of the medium was replaced with fresh medium containing GM-CSF. DCs were further incubated with 1 μg/mL lipopolysaccharide for 16 hours and then pulsed with 1 μg/mL hgp100 peptide for 3 hours to obtain mature DCs. To prepare CTLs, 1×10^7 spleen cells from pmel-1 TCR-transgenic mice were cocultured with 2×10^5 DCs in a medium containing 50 U/mL IL2 (Chiron Corporation). After 3 days of *in vitro* stimulation, approximately 90% of the harvested cells were CD3$^+$CD8$^+$ CTLs.

ACT and anti-IFNγ mAb treatment

C57BL/6 mice were inoculated subcutaneously with 1×10^6 B16 tumor cells followed by adoptive CTL transfer (1×10^7 or 4×10^7) 9 days later. Tumor growth was monitored every 2 to 3 days with calipers in an anonymous fashion. On the day of, and 2 days after, CTL transfer, mice received intraperitoneal injections of 500 μg anti-IFNγ mAb (clone XMG1.2; BioXCell) or rat IgG$_1$ isotype control (BioXCell). Tumor volume was calculated as described previously (24).

Cell preparation and flow cytometry

Tumors were harvested from mice at scheduled time points, cut into pieces, and resuspended in Hank's Balanced Salt Solution (HBSS) supplemented with 0.1% collagenase D (Roche Diagnostics) and DNase I (Roche Diagnostics) for 60 minutes at 37°C. The entire mass of the material was pressed through a 70-μm cell strainer (BD Falcon; BD Biosciences) using a plunger to obtain single-cell suspensions of tumor-infiltrating cells. For flow cytometry, the cells were first stained with the Fixable Viability Dye eFluor450 (eBioscience) to label dead cells, and pretreated with Fc Block (anti-CD16/32 clone 2.4G2; BD Pharmingen). The cells were then stained with antibodies and analyzed on a Gallios flow cytometer (Beckman Coulter). The following mAbs were obtained from BioLegend: PerCP/Cy5.5-conjugated anti-CD45, Alexa Fluor647–conjugated anti-CD90.1, and APC-Cy7–conjugated anti-CD8. Data were analyzed with the Kaluza software (Beckman Coulter).

Comprehensive gene expression analysis

Gene expression profiling data of B16 tumor tissues on different days were obtained by Agilent whole-mouse genome microarray. Total RNA was extracted with TRizol (Invitrogen) from B16 tumor tissues and fluorescently labeled using a One-Color Agilent Quick Amp Labeling Kit. The microarray slides were hybridized, washed, and read on an Agilent Microarray scanner following the manufacturer's instructions, and raw fluorescence signal intensities were generated by Agilent Feature Extraction Software v9.5. The signals were normalized to align at 75th percentile, and then turned into $\log_2$ ratio against day 1 in untreated and CTL-treated groups. We began with 45,018 probes, and removed probes if their gIsWellAboveBG flag values were 0 at all samples, and then filtered out $\log_2$ ratio values that were unvarying (between −1 and 1) at all time points. We obtained 10,855 probes and ran hierarchical clustering (standard correlation, UPGMA) on them. All data were analyzed with the Subio Platform and Basic Plug-in v1.16 (Subio Inc.). The microarray data are available from the Gene Expression Omnibus (GEO) database (series accession number GSE57304; sample accession numbers GSM1379331–GSM1379344).

For quantitative gene panel–based PCR, Cell Cycle RT^2 *Profiler* PCR arrays (SABioscience; http://www.sabiosciences.com/rt_pcr_product/HTML/PAMM-020Z.html) were used to simultaneously examine the mRNA levels of 84 genes in 96-well PCR array plates. Total RNA was prepared using TRizol according to the manufacturer's instructions (Invitrogen), and reverse-transcribed using RT2 First Strand kits (SABioscience). Real-time PCR was performed as instructed by the supplier on an ABI PRISM 7900HT Sequence Detection System (Life Technologies). Data were analyzed by a ΔΔ cycle threshold method to determine the fold changes of the mRNA levels (http://www.SABiosciences.com/pcrarraydataanalysis.php).

Expression vectors

CSII-EF-MCS/mAG-hGeminin and CSII-EF-MCS/mKO-cdt1 vectors were kindly provided by Dr. Atsushi Miyawaki (RIKEN, Wako, Japan; ref. 25). cDNA encoding mouse *IFNGR1* lacking the intracellular component of the receptor (26) was generated by PCR using the primer pair 5′-ATCTCACTCGAGATGGGCCCG-CAGGCGGCAGCT-3′ and 5′-ATCTCAGAATTCATTCTTCTTAG-TATACCAATA-3′ and subcloned into the *Xho*-1 and *Eco*-RI sites of the RV-GFP vector (designated RV-IFNGR1ΔIC; ref. 27).

Production of B16-fucci and B16-fucciΔIC tumor cells

mAG-hGeminin and mKO-cdt1 were expressed in B16 tumor cells using lentiviral vectors (designated B16-fucci). IFNGR1 lacking the sequence encoding the intracellular component of the receptor was expressed in B16-fucci tumor cells in the same way (designated B16-fucciΔIC).

Published OnlineFirst August 15, 2014; DOI: 10.1158/2326-6066.CIR-14-0098

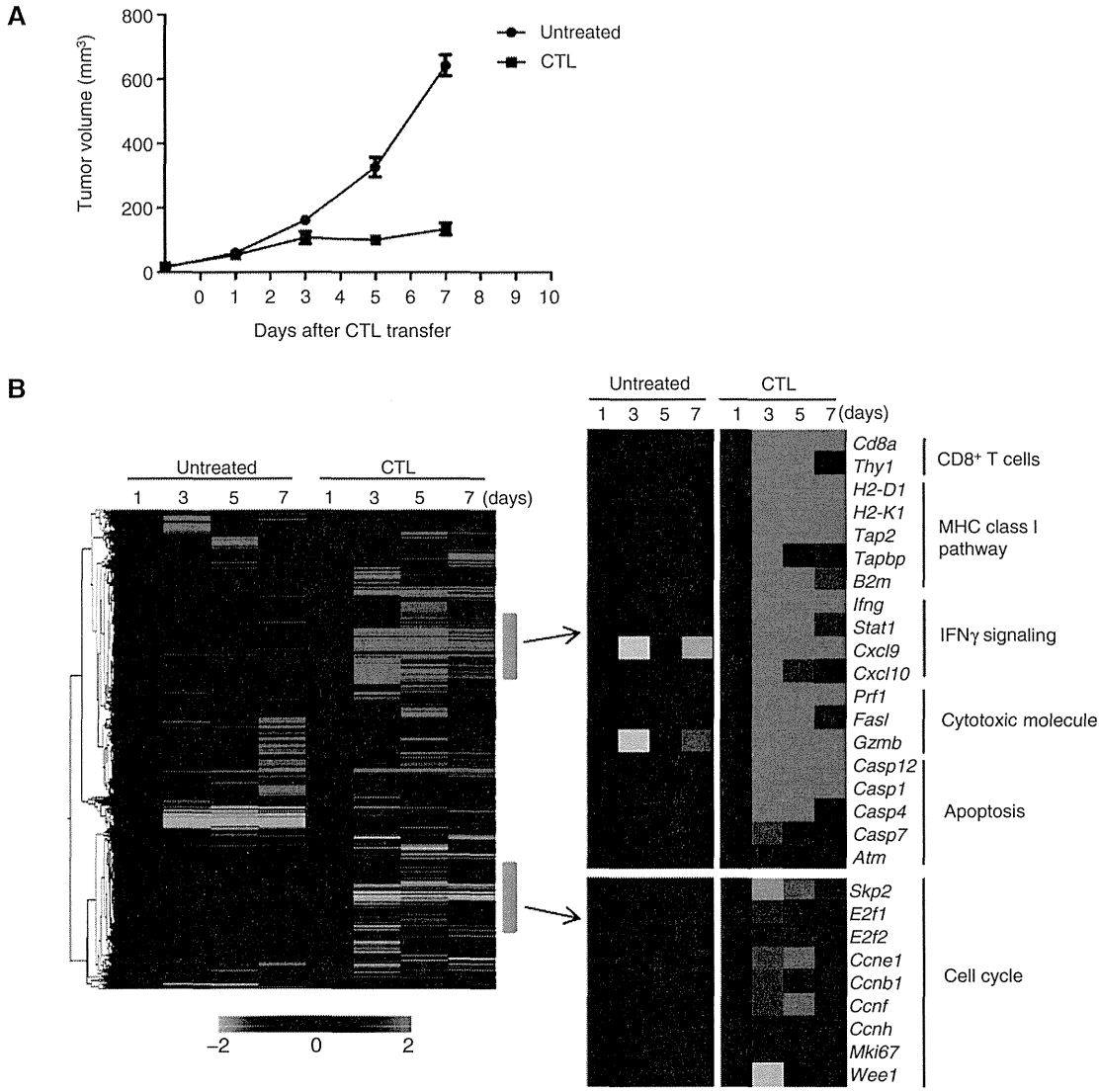

C

Genes	fold regulation	*P*
Skp2	−2.786	0.00009
E2f2	−2.7508	0.011257
Ccnb2 (Cyclin B2)	−2.1494	0.001346
Ccnf (Cyclin F)	−2.0253	0.002599
Mki67	−2.359	0.006258
Rad51	−2.3885	0.00095
Wee1	−2.4354	0.000533

Figure 1.
Gene expression analysis of the tumor in ACT. A, C57BL/6 mice were injected with 1×10^6 B16 tumor cells, and 9 days later (designated as day 0), tumor-bearing mice received 1×10^7 *in vitro* activated B16-specific (gp100-specific) CD90.1$^+$ CTLs (designated ACT mice). Tumor volumes were measured on days 1, 3, 5, and 7 after CTL transfer ($n = 5$). B, tumor tissues from untreated or ACT mice were harvested on days 1, 3, 5, and 7. Total RNA extracted from 3 to 4 tumor tissues in each group was pooled and used for gene expression analysis. Heatmaps of hierarchical clustering analysis based on fold changes of gene expression on days 3, 5, and 7 relative to day 1 are shown (left). Some groups of genes that were upregulated (top) or downregulated (bottom) after CTL transfer were extracted (right). C, cell-cycle PCR array performed using tumor tissues from untreated or ACT mice ($n = 4$) on day 3. Seven cell-cycle genes that were significantly downregulated in the tumors from ACT mice are shown. The fold regulation is the negative inverse of the fold change.

Published OnlineFirst August 15, 2014; DOI: 10.1158/2326-6066.CIR-14-0098

Quantitative RT-PCR

Total RNA was extracted using TRizol and converted into cDNA using the SuperScript III First-Strand Synthesis System according to the manufacturer's instructions (Invitrogen). Quantitative RT-PCR (qRT-PCR) reactions were carried out using EXPRESS SYBR GreenER qPCR SuperMix Universal (Invitrogen). Primer sequences are listed in Supplementary Table S1. PCR reactions were run in a Thermal Cycler Dice Real-Time System TP800 (TaKaRa) using the following program: one cycle of 95°C for 2 minutes, 40 cycles at 95°C for 15 seconds, and 60°C for 30 seconds. Results are expressed as ratios. The quantity of target mRNA was normalized to the level of GAPDH in each sample. PCR was performed in duplicate for each experiment, and PCR products were monitored by electrophoresis in 1.8% agarose gels and visualized with ethidium bromide.

Histologic analysis

Cryosections were fixed in 4% paraformaldehyde (PFA) at 4°C overnight and then transferred into 30% sucrose/PBS. After incubation for more than 24 hours, they were embedded in an optimal cutting temperature (OCT) compound (Sakura Finetek Japan) in liquid nitrogen. Sections measuring 8–10 μm were incubated with primary antibodies, followed by secondary antibodies and streptavidin. Polyclonal anti–Azami-Green antibody (PM011) was purchased from MBL. Polyclonal anti–single-stranded DNA was purchased from IBL-America. APC-conjugated anti-CD90.1 antibody was purchased from BD Biosciences. Alexa 647–conjugated polyclonal secondary antibodies and streptavidin were from Life Technologies. Anti–APC-biotin was from BioLegend. The samples were analyzed using a BZ-9000 fluorescence microscope with BZ-II image processing software (Keyence). The number of cells in the necrotic/apoptotic area was estimated by calculating the surface area of the region using BZ-H1M software (Keyence).

Cytology

Cultured B16-fucci tumor cells treated with IFNγ were examined using bright-field or fluorescence microscopy (Olympus IX71; Olympus; magnification, ×200).

Senescence-associated β-galactosidase activity assay

Senescence-associated β-galactosidase (SA-β-gal) activity in cancer cells was assessed using the Senescence Detection Kit (BioVision). SA-β-gal–positive cells were identified using bright-field microscopy (Olympus IX71; Olympus; magnification, ×400).

Protein extraction and Western blotting

B16-fucci tumors were harvested from untreated or ACT mice receiving either rat IgG (control for treatment) or anti-IFNγ mAb on day 3 after CTL transfer. Protein extracts were prepared from each tissue using RIPA buffer (Thermo Scientific) with the protease inhibitor cocktail Complete Mini (Roche). Protein extracts (50 μg) were used for immunoblotting. Protein extracts (30–50 μg) from B16-fucci, B16-fucciΔIC cells, FBL3-, or EL4-treated with IFNγ (10 U/mL) for the indicated time were used for immunoblotting. The following antibodies, all from Santa Cruz Biotechnology, were used: rabbit anti-pSTAT1 (sc-7988-R), rabbit anti-Skp2 (sc-7164), mouse anti-ATM (sc-23921), rabbit anti-p53ser15 (sc-101762), and rabbit anti-p21 (sc-397). Mouse anti-p27 (kip1) antibody was purchased from BD Biosciences. All antibodies were used at a final concentration of 0.2 to 1.0 μg/mL. After incubation with anti-rabbit IgG or anti-mouse IgG antibodies conjugated with horseradish peroxidase, proteins were visualized using the ECL Plus Western Blotting Detection System (GE Healthcare Life Sciences).

Statistical analysis

Comparison of results was performed by an unpaired, two-tailed Student *t* test with GraphPad Prism 5 (GraphPad Software, Inc.).

Results

Gene expression analysis in CTL transfer therapy

To understand the effector mechanism whereby ACT inhibits tumor growth, we assessed tumor-cell gene expression in a B16 melanoma model of pmel-1 TCR-transgenic CTL transfer. Tumors grew progressively in untreated B16-bearing mice, which was prevented between days 3 and 7 after the animals had received 10 million CTLs (Fig. 1A and Supplementary Fig. S1A). Tumor tissues were harvested from untreated mice and ACT mice on days 1, 3, 5, and 7 after CTL transfer, and gene expression was analyzed. Upregulation of genes related to $CD8^+$ T cells, the MHC class I pathway, IFNγ signaling, cytotoxic effector molecules, and others was observed in tumors from treated but not untreated mice (Fig. 1B). These data are consistent with our previous findings (24, 28) that adoptively transferred CTLs infiltrated into the tumor and that mRNA encoding *IFNγ*, *Perforin*, *Granzyme B*, and *FasL* was expressed on days 3 to 7, with kinetics reflecting the infiltration of the CTLs (Supplementary Fig. S1B and S1C).

Interestingly, some genes positively regulating the cell cycle, such as *Skp2*, *E2f2*, *Ccnf*, *Mki67*, and *Wee1*, were downregulated in tumors from ACT mice on days 3 and 5 (Fig. 1B). This was not the case in the untreated controls. We confirmed these data by a cell-cycle PCR array (Fig. 1C). Thus, gene expression analysis revealed profiles related to cell-cycle regulation, as well as cytotoxicity, in tumors from mice with ACT treatment.

CTL therapy induces G_1 cell-cycle arrest

Using the fucci (fluorescent ubiquitination-based cell-cycle indicator) system (25), we investigated the impact of ACT on the cell cycle of B16 tumor cells. To this end, we generated B16 tumor cells expressing fucci (designated B16-fucci), which emit red fluorescence in the G_1-phase, but otherwise fluoresce green. We then treated B16-fucci tumor-bearing mice with ACT. Tumor growth was not affected by the transduction of fucci into B16 tumor cells, but ACT inhibited their growth (Fig. 2A). On day 3 after CTL transfer, tumors were harvested from untreated or ACT mice for histologic analysis. As shown in Fig. 2B, CTLs had infiltrated into the tumors and were visible as blue spots. Whereas green cells were dominant in the growing tumor cells, the majority of tumor cells from ACT mice were red, suggesting that CTL therapy induced tumor cell-cycle arrest in the G_1-phase. Expressing the cell-cycle state as a green:red (G:R) ratio (Fig. 2C) showed that this was lower in the ACT mice (0.26 ± 0.12; $n = 3$) than in the untreated control mice on day 3 (1.1 ± 0.05; $n = 3$; $P = 0.0032$). This difference remained up to day 5 after CTL transfer, but on day 7, the G:R ratio increased again, together with the disappearance of CTLs, and green cells became dominant once more after day 10 (Supplementary Fig. S1B).

Published OnlineFirst August 15, 2014; DOI: 10.1158/2326-6066.CIR-14-0098

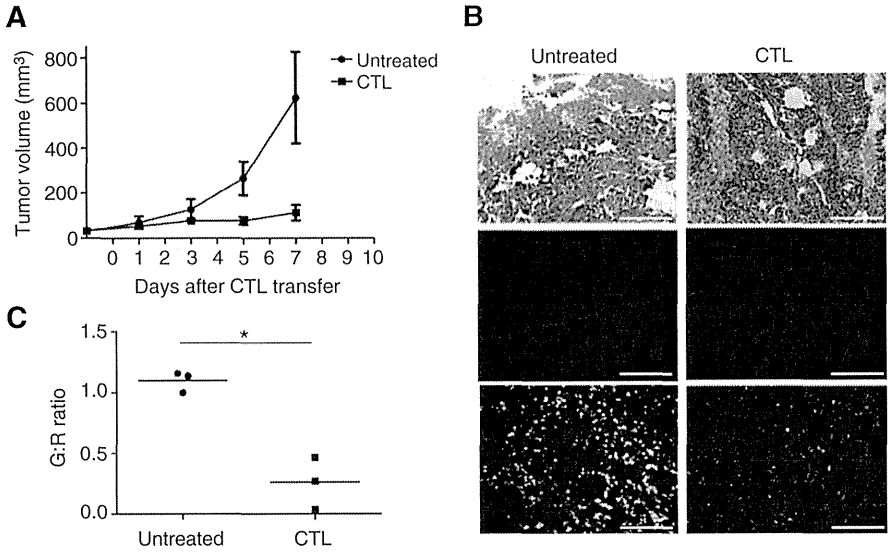

Figure 2.
CTL transfer therapy induced G_1 cell-cycle arrest of the tumor. A, C57BL/6 mice were injected with 1×10^6 B16-fucci tumor cells, and 9 days later, tumor-bearing mice ($n = 5$) were treated as described in Fig. 1. B, representative hematoxylin and eosin (top) and fluorescence microscopy images (middle and bottom) of cryosections of B16-fucci on day 3 ($n = 3$ per group). Alexa Fluor647–labeled anti-mouse CD90.1 antibody was used to detect infiltrating CD90.1$^+$ T cells (blue cells; middle). Scale bars, 200 μm. C, analysis of cell-cycle stage was performed by calculating the G:R ratio in fluorescence images ($n = 3$ per group). Samples were compared using an unpaired, two-tailed Student t test (*, $P < 0.01$).

IFNγ is critical for tumor growth inhibition and cell-cycle arrest

IFNγ is important for antitumor immunity. We have shown that it is critical for tumor growth inhibition in this model using IFNγ neutralizing antibody (anti-IFNγ mAb; ref. 28). Because IFNγ is involved in MHC class I upregulation, antigen processing, and trafficking of T cells into the tumor site by promoting chemokine production, the number of T cells infiltrating into the tumor was decreased by neutralizing IFNγ (data not shown). It was necessary to inject 4-fold more T cells to achieve the same level of CTL infiltration in anti-IFNγ Ab-treated animals (Fig. 3B). Nevertheless, anti-IFNγ treatment still prevented tumor growth blockade, despite the presence of equivalent levels of CTL in the tumor (Fig. 3A). Strikingly, this was the case even though the expression of mRNA encoding the effector molecules *IFNγ*, *Perforin*, *Granzyme B*, and *FasL* in ACT mice treated with anti-IFNγ mAb was the same or even higher than that in control ACT mice treated with rat IgG (Fig. 3C and D). A major difference in the anti-IFNγ mAb-treated mice was that the expression of mRNA encoding *STAT1* and IFNγ-inducible genes such as *MIG*, *IP10*, or *I-TAC* was suppressed. This suggests that IFNγ signaling was blocked by the treatment with anti-IFNγ mAb.

As shown in Fig. 4A, all tumor cells fluoresced either green or red. In growing tumors, the majority of B16 tumor cells were in the S–G_2–M phase (Fig. 4A, left). After CTL transfer, most of the tumor cells became red (Fig. 4A, middle), but in the anti-IFNγ mAb-treated ACT mice, the tumor cells remained green (Fig. 4A, right). Diffused infiltration of CTLs into the tumor accompanied by massively infiltrated mononuclear cells and destruction of tumor cells, corresponding to spotty necrotic/apoptotic areas, was seen in ACT mice whether or not they received anti-IFNγ mAb treatment. Furthermore, apoptotic cells positive for single-stranded DNA (ssDNA), detected as white spots, were rare, but were present equally in ACT mice with or without anti-IFNγ mAb treatment (Fig. 4B and C). This, therefore, suggests that the transferred CTLs actually mediated relatively little tumor cell killing, which was unaffected by anti-IFNγ mAb administration.

The numbers of CTLs, tumor cells in necrotic/apoptotic areas, and tumor cells in the G_1 or S–G_2–M phase were compared systematically in these mice. More green than red cells were observed in untreated tumors (Fig. 4D). In CTL-treated tumors, as described above, the G:R ratio was inverted, but the ratio was restored by the abrogation of IFNγ signaling. The surface area of the part of the tumor with necrotic/apoptotic cells was similar in the two CTL-treated groups (with or without anti-IFNγ mAb treatment), and the estimated number of dead cells was always smaller than that of the live cells (whether green or red; Fig. 4E). These results indicate that G_1 cell-cycle arrest, and not cytolytic killing, was primarily responsible for the CTL-induced suppression of tumor growth.

IFNγ directly suppress B16-fucci tumor cell growth through cell-cycle arrest

We constructed B16-fucci tumor cells expressing an IFNγ receptor lacking the intracellular component (B16-fucciΔIC). ACT did not suppress the growth of these cells even when 4-fold more CTLs (4×10^7) were transferred (Supplementary Fig. S2A). Although a similar number of CTLs infiltrated into B16-fucciΔIC tumor sites, as in mice with B16-fucci tumors receiving 4-fold less CTLs, no IFNγ production was observed (Supplementary Fig. S2B and S2C), and therefore the effect of IFNγ could not be evaluated in this system. This might be due to limited recognition of B16-fucciΔIC tumor cells by the CTL, because of their low level of MHC class I expression (Supplementary Fig. S2D). As expected, B16-fucciΔIC did not upregulate MHC class I molecules after exposure to IFNγ.

Because we could not evaluate the effect of IFNγ on tumor cells *in vivo* in this manner, we tested its effects directly on B16 tumor cells *in vitro*. As shown in Fig. 5, proliferation of B16-fucci cells, but not B16-fucciΔIC cells, was inhibited completely when they were treated with IFNγ (Fig. 5A). These cells were arrested in G_1 (Fig. 5B), showing that IFNγ directly inhibits the growth of B16-fucci tumor cells through G_1 cell-cycle arrest.

Recently, it was reported that a combination of IFNγ and TNFα produced by CD4$^+$ T cells can drive tumor cells into senescence by inducing G_0–G_1 cell-cycle arrest through the activation of p16INK4a (14). Therefore, we tested the effect of IFNγ and/or

Published OnlineFirst August 15, 2014; DOI: 10.1158/2326-6066.CIR-14-0098

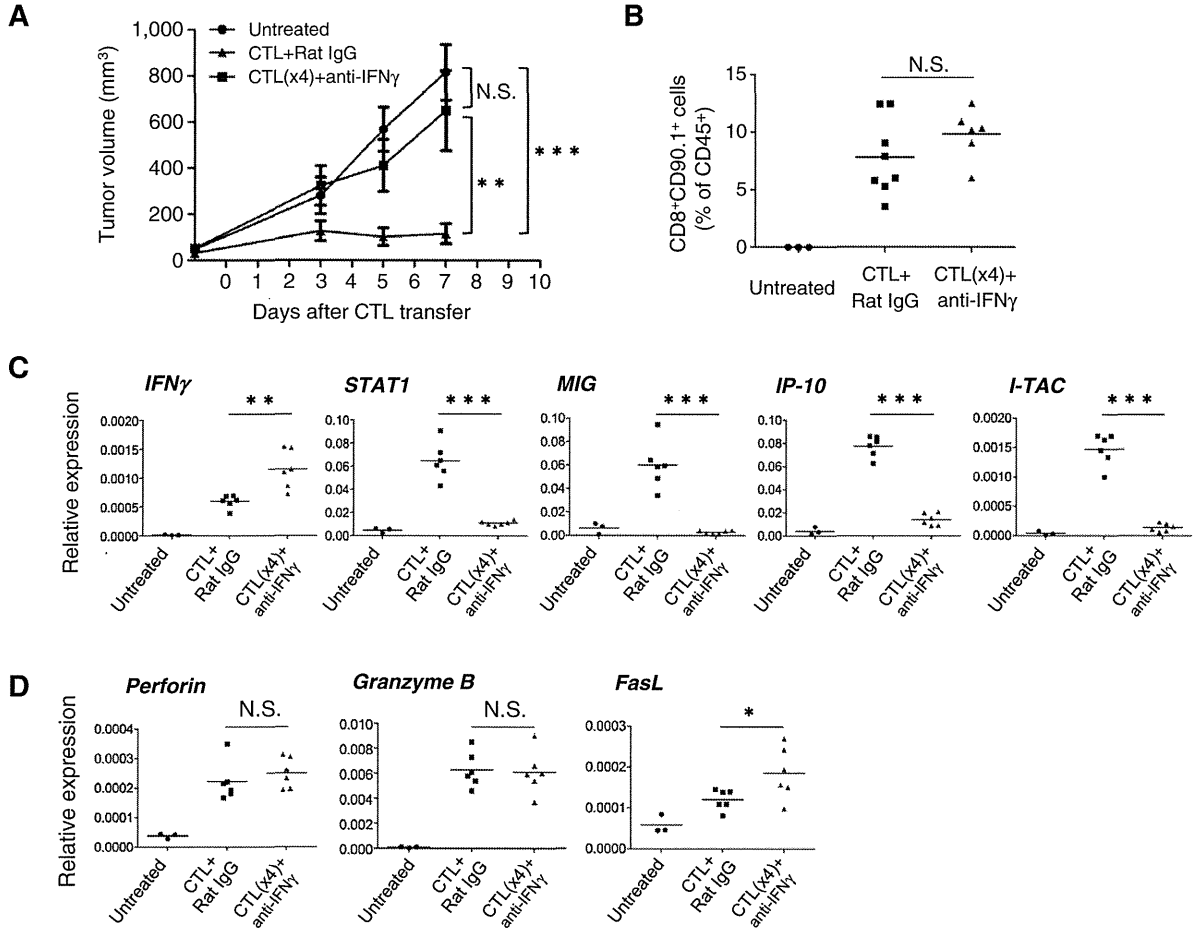

Figure 3.

IFNγ is critical for tumor growth inhibition. A, C57BL/6 mice were injected with B16-fucci tumor cells. Tumor-bearing mice ($n = 5$) were treated as described in Fig. 1, and anti-IFNγ or control rat IgG antibodies were injected intraperitoneally on days 0 and 2 after CTL transfer. Tumor volumes were measured on days 3, 5, and 7 after CTL transfer ($n = 5$). B, the frequency of CTLs ($CD45^+$ $CD90.1^+$ $CD8^+$) was assessed by flow cytometry. Tumors were harvested from each group on day 3 after CTL transfer. C and D, total RNA was isolated from tumor tissues and reverse-transcribed into cDNA. Expression of IFNγ-related genes (*IFNγ*, *STAT1*, *MIG*, *IP-10*, and *I-TAC*; C) and cytotoxicity-related genes (*Perforin*, *Granzyme B*, and *FasL*; D) was determined by qRT-PCR. *GAPDH* was used as an internal control. Samples were compared using an unpaired, two-tailed Student *t* test (*, $P < 0.05$; **, $P < 0.01$; and ***, $P < 0.001$; N.S., not statistically significant).

TNFα on B16 tumor cells. Whereas IFNγ alone inhibited cell proliferation by G_1 arrest, TNFα alone had a limited inhibitory effect on B16 proliferation even at a high concentration (10 ng/mL; Supplementary Fig. S3). When B16 tumor cells were cultured in the presence of both IFNγ and TNFα at a high concentration, a synergistic effect on cell growth inhibition and cell senescence was observed (Supplementary Fig. S3).

IFNγ production by transferred CTLs induces G_1 cell-cycle arrest by a mechanism involving Skp2/p27-related cell-cycle regulation

We next investigated the mechanism of G_1 cell-cycle arrest by IFNγ. B16-fucci tumor tissues were harvested from untreated mice, ACT mice treated with rat IgG, or ACT mice treated with anti-IFNγ mAb on day 3 after CTL transfer. Proteins were extracted from each tissue for Western blot analysis. As shown in Fig. 6A, downstream of IFNγ signaling, STAT1 was phosphorylated in tumors from ACT mice treated with rat IgG, but not in tumors from anti-IFNγ mAb-treated ACT mice. To confirm the gene expression data that *Skp2* was significantly downregulated in tumors from ACT mice (Fig. 1B and C), we examined the protein expression of Skp2. As shown in Fig. 6A, Skp2 expression was suppressed in tumors from control ACT mice, but not in those from mice treated with anti-IFNγ mAb. Conversely, the cyclin-dependent kinase inhibitor (CKI) p27 accumulated in the former but not in the latter. We also investigated the ataxia telangiectasia mutated (ATM)–p53–p21 pathway involved in G_1 cell-cycle arrest following DNA damage. We found that ATM was not upregulated as a result of CTL therapy, p53 was not activated, and no subsequent accumulation of p21 was observed. This shows that the ATM–p53–p21 pathway is not involved in this model (Fig. 6A). We also investigated the expression of these molecules *in vitro* (Fig. 6B). B16-fucci and B16-fucciΔIC tumor cells were treated with 10 U/mL IFNγ and

Published OnlineFirst August 15, 2014; DOI: 10.1158/2326-6066.CIR-14-0098

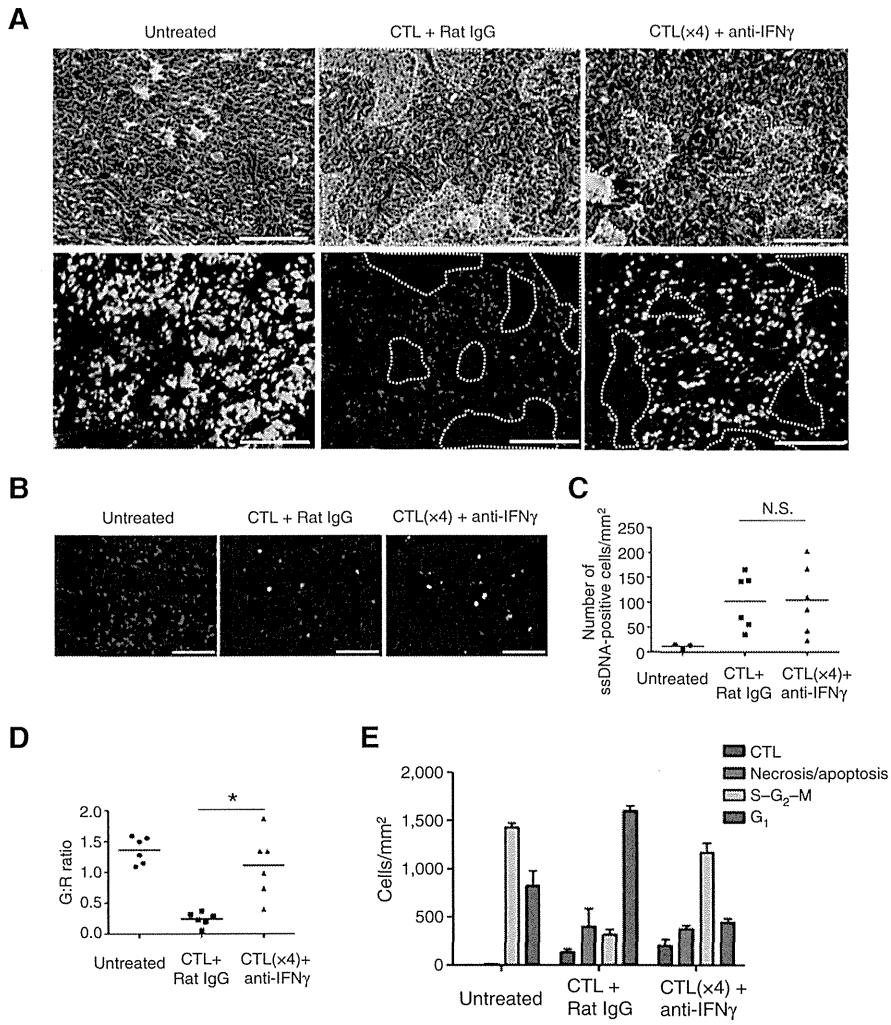

Figure 4.
CTLs block tumor growth by both lytic activity and IFNγ-dependent cell-cycle arrest. A, B16-fucci tumor-bearing mice ($n = 3$) were treated as described in Fig. 3. Hematoxylin and eosin (top) and fluorescence microscopy images (bottom) of frozen tumor sections on day 3 are shown. Dotted yellow lines, necrotic areas. Scale bars, 200 μm. B, apoptotic cells positive for ssDNA are shown in fluorescence microscopy images on day 3. Cells were counterstained with DAPI. Scale bars, 100 μm. C, quantification of ssDNA-positive cells within tumors. Numbers of ssDNA-positive cells were counted in five random fields of view. Data are expressed as the means ± SE of untreated mice ($n = 3$) and ACT mice injected with rat IgG ($n = 6$) or anti-IFNγ mAb ($n = 6$). D, analysis of the cell cycle was performed by calculating the G:R ratio in fluorescence images ($n = 6$ per group). E, the number of CTLs, tumor cells in necrotic areas, and tumor cells in G_1 or S–G_2–M. The number of cells in necrotic areas was estimated by calculating the surface area of the region using BZ-HIM software (Keyence). Total number of cells in at least three random fields of view (per mm^2) is shown. Representative data of 3 mice for each group are given. Samples were compared using an unpaired, two-tailed Student t test (*, $P < 0.01$; N.S., not statistically significant).

harvested at the indicated times. STAT1 phosphorylation was observed at early time points (15 and 30 minutes after IFNγ treatment) in B16-fucci, but not in B16-fucciΔIC. Skp2 expression was downregulated gradually, and p27 accumulated by 48 hours after IFNγ treatment in B16-fucci but not in B16-fucciΔIC cells (Fig. 6B). We confirmed that the ATM–p53–p21 pathway was also not involved in G_1 cell-cycle arrest *in vitro*. These results suggest that G_1 cell-cycle arrest by CTL therapy is likely due to Skp2/p27-related cell-cycle regulation by IFNγ.

Inhibition of FBL3 cell proliferation by IFNγ

We next investigated whether proliferation of other murine cell lines is inhibited by IFNγ. FBL3, p815, CT26, 3LL, and EL4 tumor cells were treated with IFNγ (10 U or 100 U/mL) for 4 to 6 days (Fig. 7A). The proliferation of FBL3 tumor cells was inhibited by IFNγ treatment in a manner similar to that of B16 tumor cells. The proliferation of P815, CT26, and 3LL tumor cells was moderately inhibited. No inhibition was observed in IFNγ-treated EL4 tumor cells. In Western blot analyses, using tumor lysates from FBL3 and EL4 tumors at the indicated time point, Stat1 phosphorylation was observed in FBL3 lysates, but the phosphorylation was very weak in EL4 tumor lysates. Skp2 expression was downregulated 24 to 48 hours after IFNγ treatment in FBL3 but not in EL4 tumors, and p27 accumulated (Fig. 7B). Again, the ATM–p53–p21 pathway was not involved. These results suggest that inhibition of FBL3 tumor cell proliferation by IFNγ might involve Skp2/p27-related cell-cycle regulation, as in B16.

Discussion

In this study, we demonstrated that the mechanism of tumor growth inhibition by adoptive CTL therapy was largely dependent on IFNγ-induced G_1 cell-cycle arrest rather than on tumor cell lysis. In microarray analysis, the upregulation of genes related to $CD8^+$ T cells, the MHC class I pathway, IFNγ signaling, cytotoxic effector molecules, and others was observed in tumors from ACT mice. At the same time, a decrease was found in the expression of some genes positively regulating the cell cycle in these tumors. Therefore, we focused on cell-cycle control in the B16 adoptive immunotherapy model and used the fucci system, which allows the visualization of cell-cycle stage of tumor cells *in situ* in mice receiving CTL.

Published OnlineFirst August 15, 2014; DOI: 10.1158/2326-6066.CIR-14-0098

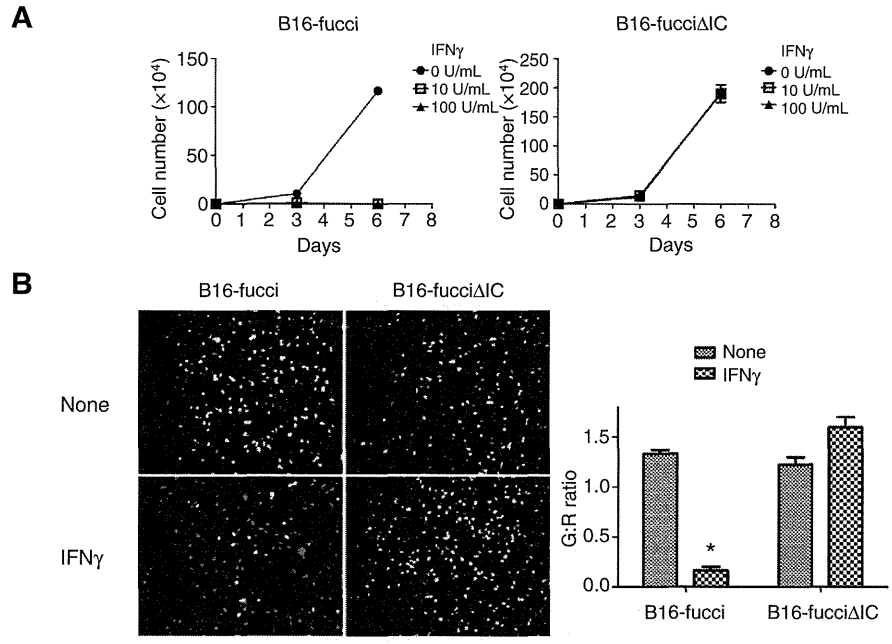

Figure 5.
IFNγ directly inhibits tumor cell growth through G_1 cell-cycle arrest. A, proliferation of B16-fucci cells or B16-fucci expressing an IFNγ receptor lacking the intracellular component (B16-fucciΔIC) was assessed after exposure to IFNγ (10 U/mL) for 6 days. B, B16-fucci or B16-fucciΔIC cells were incubated with IFNγ (10 U/mL). Two days later, the cell-cycle state was determined by fluorescence microscopy (left). Original magnification, ×200. The G:R ratio in fluorescence images is shown ($n = 2$ per group; right). Samples were compared using an unpaired, two-tailed Student t test (*, $P < 0.01$).

Histologic analysis following ACT showed that the number of CTLs in the tumor was far lower than that of tumor cells. On average, only 140 CTLs per mm^2 tumor tissue on day 3 after transfer were found. In contrast, this area contained 1,911 tumor cells (both green and red cells). Thus, it seems *a priori* unlikely that this small number of CTLs infiltrating the tumor would be sufficient to prevent tumor growth by direct cytotoxicity 3 to 7 days after CTL injection. Consistent with this observation, we also found that the area of the tumor undergoing necrosis/apoptosis was relatively small. Instead, a larger area consisting of tumor cells had undergone cell-cycle arrest at G_1. Therefore, transient tumor suppression from days 3 to 7 seems to be largely due to cell-cycle arrest rather than due to CTL killing. Using mAbs that neutralize IFNγ and completely block IFNγ signaling, we demonstrated that IFNγ is required for tumor growth inhibition and G_1 cell-cycle arrest but not for CTL killing. Thus, IFNγ-dependent G_1 cell-cycle arrest makes a major contribution to tumor growth suppression in this model. This would explain why tumor growth was suppressed despite the low ratio of CTLs to tumor cells in this system, and how T cells can suppress the growth of bystander tumor cells that may not express the target antigen. This could also explain some examples to tumor suppression by $CD4^+$ T cells that can also make IFNγ even if they are not lytic and even if the tumor is MHC class II negative, as long as antigen-presenting cells are infiltrating and can present antigen, as the soluble IFNγ can target neighboring cells.

IFNγ inhibits cell proliferation via cell type–specific pathways that involve CKIs, such as p21Cip1 (29, 30) and p27Kip1 (31, 32). It has been shown that STAT1 interacts directly with cyclin D1/Cdk4 and mediates the cell-cycle arrest of human U3A cells (33). Here, we investigated the involvement of CKIs in G_1 cell-cycle arrest, and found that p27Kip1, but not p21Cip1, accumulated in B16 tumor cells following CTL therapy *in vivo* or IFNγ treatment *in vitro*. Another CKI, p16, is involved in senescence-like G_1 cell-cycle arrest (14), but this factor is not expressed in B16 tumor cells due to a $p16^{Ink4a}$ exon1α deletion (34). Thus, p27Kip1 appeared to be the major CKI involved in G_1 arrest in this model. *Skp2* is an oncogene; Skp2 inactivation induces cell senescence independent

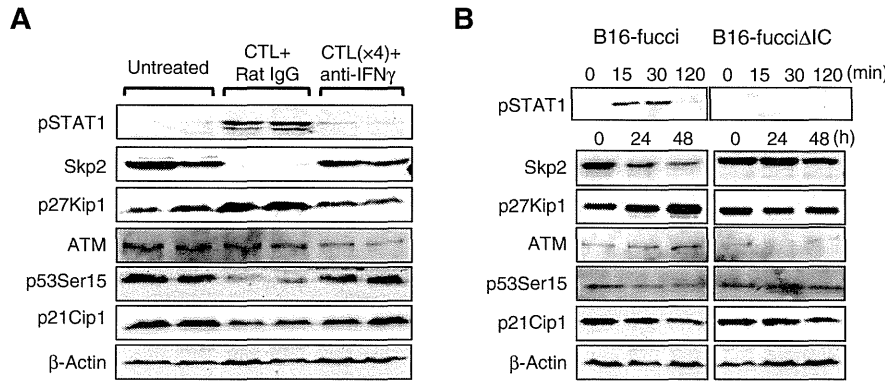

Figure 6.
G_1 cell-cycle arrest by ACT was mediated by IFNγ-dependent Skp2/p27-related cell-cycle regulation. A, B16-fucci tumors were harvested from untreated or ACT mice given control rat IgG or anti-IFNγ mAb on day 3 after CTL transfer. Protein extracts (50 μg) from tumor tissues in each group were used for immunoblotting of the indicated proteins. B, protein extracts from B16-fucci or B16-fucciΔIC cells treated with IFNγ (10 U/mL) for the indicated time were used for immunoblotting of the indicated proteins.

Published OnlineFirst August 15, 2014; DOI: 10.1158/2326-6066.CIR-14-0098

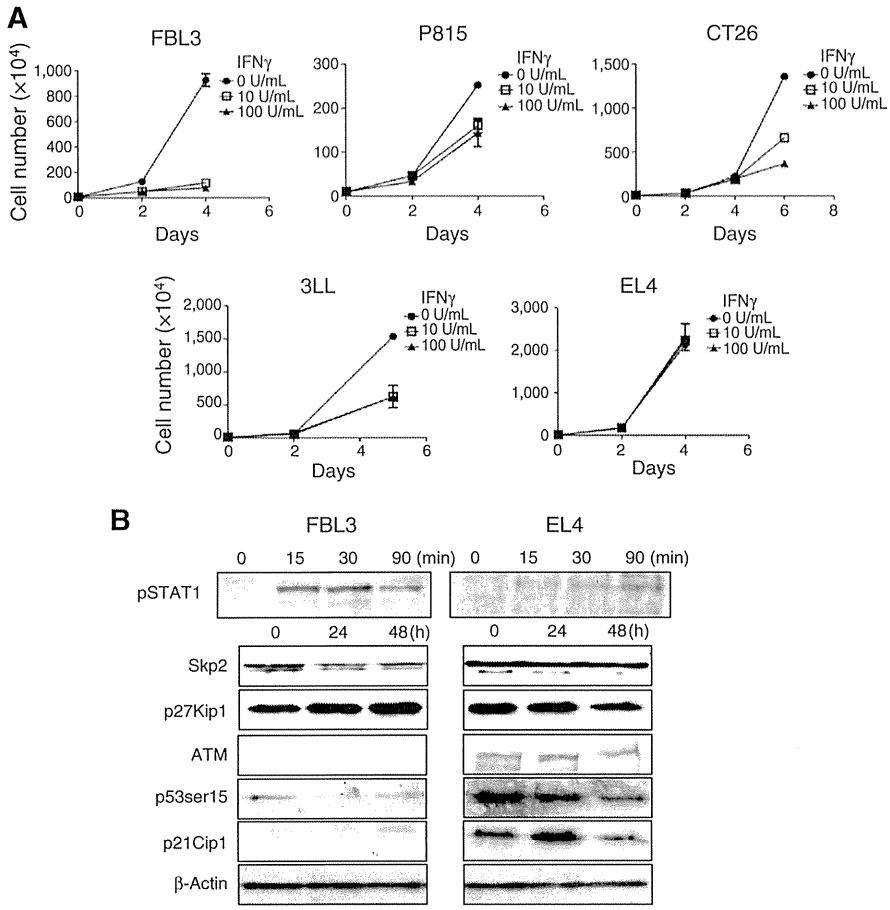

Figure 7.
Inhibition of cell proliferation by IFNγ in other murine cell lines. A, proliferation of FBL3, P815, CT26, 3LL, and EL4 cells after treatment with IFNγ (10 or 100 U/mL) for 4 to 6 days. B, protein extracts from FBL3 and EL4 cells treated with IFNγ (10 U/mL) for the indicated time were used for immunoblotting of the indicated proteins.

of the p53 pathway (35). STAT1 has been shown to repress *Skp2* gene transcription by binding to its promoter region and stabilizing p27Kip1 in Ras-transformed cells (36). In this report, we showed that Skp2 expression was downregulated after either CTL therapy or IFNγ treatment; thus, STAT1 may repress Skp2 expression and promote p27Kip1 stabilization.

G_1 cell-cycle arrest is also known to be induced by ATM-dependent activation of p53 and induction of p21Cip1 (37). Because ATM is a key molecule in the cellular response to DNA damage (38), we investigated its expression by Western blot analysis. We found that the ATM protein was not highly expressed in the tumor after CTL therapy. We also confirmed this finding *in vitro* in B16 cells cultured with IFNγ. Furthermore, p53 was not phosphorylated at Ser15, and the CKI p21Cip1, which is downstream of phospho-p53 (Ser15), was not upregulated. Therefore, we conclude that ATM expression and the subsequent activation of the phospho-p53–p21 pathway was not involved in this model.

We tested the effect of IFNγ on other murine tumor cell lines, and found that the proliferation of FBL-3 cells was strongly inhibited by IFNγ, similar to that of the B16 tumor cells. On the other hand, EL-4 cells were insensitive to IFNγ, whereas p815, CT26, and 3LL cells were moderately sensitive. IFNγ sensitivity and the mechanisms involved in the inhibition of cell proliferation may differ in different tumor cell lines. It is important to know whether IFNγ insensitivity is due to the downregulation of IFNγ receptors on these tumors, or defects in their IFNγ signal transduction.

Braumuller and colleagues (14) reported that IFNγ together with TNFα reduced the proliferation of different cancer cell lines in both mice and humans. Here, we showed that the combination of IFNγ and TNFα strongly inhibited B16 tumor cell proliferation and induced cell senescence (Supplementary Fig. S3). Because pmel-1 CTLs produce large amounts of IFNγ, but not TNFα, when they are cultured with B16 tumor cells *in vitro* (Supplementary Fig. S4), and IFNγ alone is enough to suppress tumor cell proliferation (Supplementary Fig. S3), the transient suppression of tumor growth from days 3 to 7 *in vivo* in this model may be entirely due to IFNγ, as there is only a small amount of TNFα at the tumor site. Th1 $CD4^+$ T cells or Toll-like receptor (TLR)–stimulated macrophages might be able to produce enough TNFα, but these cells are not present in our system. Alternatively, a strategy to induce polyfunctional $CD8^+$ T cells producing IFNγ, TNFα, and IL2 might be important to enhance further the antitumor effects in this model (39, 40).

IFNγ is a critical molecule in cancer immunosurveillance or immunoediting in primary mouse tumor models (41–44). In our study, as long as high concentrations of IFNγ were present

Published OnlineFirst August 15, 2014; DOI: 10.1158/2326-6066.CIR-14-0098

in the tumor, its growth was controlled through G_1 arrest (Supplementary Fig. S1). Thus, our study suggests that deregulation of the cell cycle due to insufficient availability of IFNγ or IFNγ insensitivity developed by tumor cells may be one mechanism by which tumor cells escape from CTL therapy (Supplementary Figs. S1 and S2).

Our study indicates that a small number of infiltrated CTLs can cause a large number of tumor cells to arrest in G_1 rather than dying. On the basis of this finding, we propose that the development of an appropriate strategy to maintain tumor cells in a quiescent, dormant state for extended periods (immunotherapy-induced equilibrium/dormancy), or to induce apoptosis/senescence, would be highly desirable.

Disclosure of Potential Conflicts of Interest

No potential conflicts of interest were disclosed.

Authors' Contributions

Conception and design: H. Matsushita, R. Maekawa, K. Kakimi
Development of methodology: M. Tomura, K. Kakimi
Acquisition of data (provided animals, acquired and managed patients, provided facilities, etc.): H. Matsushita, A. Hosoi, S. Ueha, J. Abe, N. Fujieda, R. Maekawa, O. Ohara, K. Kakimi
Analysis and interpretation of data (e.g., statistical analysis, biostatistics, computational analysis): H. Matsushita, A. Hosoi, S. Ueha, N. Fujieda, O. Ohara, K. Kakimi
Writing, review, and/or revision of the manuscript: H. Matsushita, K. Kakimi
Administrative, technical, or material support (i.e., reporting or organizing data, constructing databases): O. Ohara
Study supervision: K. Matsushima, K. Kakimi

Acknowledgments

The authors thank Dr. N. Restifo (National Cancer Institute) for providing the B16F10 tumor cell line, Dr. A. Miyawaki (RIKEN, Wako) for the Fucci system, and Mr. K. Sato (Kazusa DNA Research Institute) for excellent technical assistance in gene expression analysis.

Grant Support

This study was supported in part by a Grant-in-Aid for Scientific Research of the Ministry of Education, Culture, Sports, Science and Technology of Japan (K. Kakimi).

The costs of publication of this article were defrayed in part by the payment of page charges. This article must therefore be hereby marked *advertisement* in accordance with 18 U.S.C. Section 1734 solely to indicate this fact.

Received May 16, 2014; revised July 22, 2014; accepted August 5, 2014; published OnlineFirst August 15, 2014.

References

1. Rosenberg SA, Restifo NP, Yang JC, Morgan RA, Dudley ME. Adoptive cell transfer: a clinical path to effective cancer immunotherapy. Nat Rev Cancer 2008;8:299–308.
2. Morgan RA, Dudley ME, Wunderlich JR, Hughes MS, Yang JC, Sherry RM, et al. Cancer regression in patients after transfer of genetically engineered lymphocytes. Science 2006;314:126–9.
3. Brenner MK, Heslop HE. Adoptive T cell therapy of cancer. Curr Opin Immunol 2010;22:251–7.
4. Kalos M, Levine BL, Porter DL, Katz S, Grupp SA, Bagg A, et al. T cells with chimeric antigen receptors have potent antitumor effects and can establish memory in patients with advanced leukemia. Sci Transl Med 2011;3:95ra73.
5. Robbins PF, Morgan RA, Feldman SA, Yang JC, Sherry RM, Dudley ME, et al. Tumor regression in patients with metastatic synovial cell sarcoma and melanoma using genetically engineered lymphocytes reactive with NY-ESO-1. J Clin Oncol 2011;29:917–24.
6. Vierboom MP, Nijman HW, Offringa R, van der Voort EI, van Hall T, van den Broek L, et al. Tumor eradication by wild-type p53-specific cytotoxic T lymphocytes. J Exp Med 1997;186:695–704.
7. Hanson HL, Donermeyer DL, Ikeda H, White JM, Shankaran V, Old LJ, et al. Eradication of established tumors by CD8+ T cell adoptive immunotherapy. Immunity 2000;13:265–76.
8. Mukherjee P, Ginardi AR, Tinder TL, Sterner CJ, Gendler SJ. MUC1-specific cytotoxic T lymphocytes eradicate tumors when adoptively transferred *in vivo*. Clin Cancer Res 2001;7:848s–55s.
9. Kagi D, Vignaux F, Ledermann B, Burki K, Depraetere V, Nagata S, et al. Fas and perforin pathways as major mechanisms of T cell-mediated cytotoxicity. Science 1994;265:528–30.
10. Spiotto MT, Rowley DA, Schreiber H. Bystander elimination of antigen loss variants in established tumors. Nat Med 2004;10:294–8.
11. Breart B, Lemaitre F, Celli S, Bousso P. Two-photon imaging of intratumoral CD8+ T cell cytotoxic activity during adoptive T cell therapy in mice. J Clin Invest 2008;118:1390–7.
12. Zhang B, Karrison T, Rowley DA, Schreiber H. IFN-gamma- and TNF-dependent bystander eradication of antigen-loss variants in established mouse cancers. J Clin Invest 2008;118:1398–404.
13. Muller-Hermelink N, Braumuller H, Pichler B, Wieder T, Mailhammer R, Schaak K, et al. TNFR1 signaling and IFN-gamma signaling determine whether T cells induce tumor dormancy or promote multistage carcinogenesis. Cancer Cell 2008;13:507–18.
14. Braumuller H, Wieder T, Brenner E, Assmann S, Hahn M, Alkhaled M, et al. T-helper-1-cell cytokines drive cancer into senescence. Nature 2013;494:361–5.
15. Dunn GP, Koebel CM, Schreiber RD. Interferons, immunity and cancer immunoediting. Nat Rev Immunol 2006;6:836–48.
16. Winter H, Hu HM, McClain K, Urba WJ, Fox BA. Immunotherapy of melanoma: a dichotomy in the requirement for IFN-gamma in vaccine-induced antitumor immunity versus adoptive immunotherapy. J Immunol 2001;166:7370–80.
17. Liao F, Rabin RL, Yannelli JR, Koniaris LG, Vanguri P, Farber JM. Human Mig chemokine: biochemical and functional characterization. J Exp Med 1995;182:1301–14.
18. Luster AD, Leder P. IP-10, a -C-X-C- chemokine, elicits a potent thymus-dependent antitumor response *in vivo*. J Exp Med 1993;178:1057–65.
19. Cole KE, Strick CA, Paradis TJ, Ogborne KT, Loetscher M, Gladue RP, et al. Interferon-inducible T cell alpha chemoattractant (I-TAC): a novel non-ELR CXC chemokine with potent activity on activated T cells through selective high affinity binding to CXCR3. J Exp Med 1998;187:2009–21.
20. Bromberg JF, Horvath CM, Wen Z, Schreiber RD, Darnell JE Jr. Transcriptionally active Stat1 is required for the antiproliferative effects of both interferon alpha and interferon gamma. Proc Natl Acad Sci U S A 1996;93:7673–8.
21. Chin YE, Kitagawa M, Su WC, You ZH, Iwamoto Y, Fu XY. Cell growth arrest and induction of cyclin-dependent kinase inhibitor p21 WAF1/CIP1 mediated by STAT1. Science 1996;272:719–22.
22. Meurs E, Chong K, Galabru J, Thomas NS, Kerr IM, Williams BR, et al. Molecular cloning and characterization of the human double-stranded RNA-activated protein kinase induced by interferon. Cell 1990;62:379–90.
23. Deiss LP, Feinstein E, Berissi H, Cohen O, Kimchi A. Identification of a novel serine/threonine kinase and a novel 15-kD protein as potential mediators of the gamma interferon-induced cell death. Genes Dev 1995;9:15–30.
24. Noji S, Hosoi A, Takeda K, Matsushita H, Morishita Y, Seto Y, et al. Targeting spatiotemporal expression of CD137 on tumor-infiltrating cytotoxic T lymphocytes as a novel strategy for agonistic antibody therapy. J Immunother 2012;35:460–72.
25. Sakaue-Sawano A, Kurokawa H, Morimura T, Hanyu A, Hama H, Osawa H, et al. Visualizing spatiotemporal dynamics of multicellular cell-cycle progression. Cell 2008;132:487–98.

Published OnlineFirst August 15, 2014; DOI: 10.1158/2326-6066.CIR-14-0098

26. Dighe AS, Richards E, Old LJ, Schreiber RD. Enhanced *in vivo* growth and resistance to rejection of tumor cells expressing dominant negative IFN gamma receptors. Immunity 1994;1:447–56.
27. Ranganath S, Ouyang W, Bhattarcharya D, Sha WC, Grupe A, Peltz G, et al. GATA-3-dependent enhancer activity in IL-4 gene regulation. J Immunol 1998;161:3822–6.
28. Hosoi A, Matsushita H, Shimizu K, Fujii SI, Ueha S, Abe J, et al. Adoptive cytotoxic T lymphocyte therapy triggers a counter-regulatory immunosuppressive mechanism via recruitment of myeloid-derived suppressor cells. Int J Cancer 2014;134:1810–22.
29. Hobeika AC, Etienne W, Torres BA, Johnson HM, Subramaniam PS. IFN-gamma induction of p21(WAF1) is required for cell cycle inhibition and suppression of apoptosis. J Interferon Cytokine Res 1999;19:1351–61.
30. Gooch JL, Herrera RE, Yee D. The role of p21 in interferon gamma-mediated growth inhibition of human breast cancer cells. Cell Growth Differ 2000;11:335–42.
31. Harvat BL, Seth P, Jetten AM. The role of p27Kip1 in gamma interferon-mediated growth arrest of mammary epithelial cells and related defects in mammary carcinoma cells. Oncogene 1997;14:2111–22.
32. Lee SH, Kim JW, Oh SH, Kim YJ, Rho SB, Park K, et al. IFN-gamma/IRF-1-induced p27kip1 down-regulates telomerase activity and human telomerase reverse transcriptase expression in human cervical cancer. FEBS Lett 2005;579:1027–33.
33. Dimco G, Knight RA, Latchman DS, Stephanou A. STAT1 interacts directly with cyclin D1/Cdk4 and mediates cell cycle arrest. Cell Cycle 2010;9:4638–49.
34. Melnikova VO, Bolshakov SV, Walker C, Ananthaswamy HN. Genomic alterations in spontaneous and carcinogen-induced murine melanoma cell lines. Oncogene 2004;23:2347–56.
35. Lin HK, Chen Z, Wang G, Nardella C, Lee SW, Chan CH, et al. Skp2 targeting suppresses tumorigenesis by Arf-p53-independent cellular senescence. Nature 2010;464:374–9.
36. Wang S, Raven JF, Koromilas AE. STAT1 represses Skp2 gene transcription to promote p27Kip1 stabilization in Ras-transformed cells. Mol Cancer Res 2010;8:798–805.
37. Delia D, Fontanella E, Ferrario C, Chessa L, Mizutani S. DNA damage-induced cell-cycle phase regulation of p53 and p21waf1 in normal and ATM-defective cells. Oncogene 2003;22:7866–9.
38. Kitagawa R, Kastan MB. The ATM-dependent DNA damage signaling pathway. Cold Spring Harb Symp Quant Biol 2005;70:99–109.
39. Perret R, Ronchese F. Effector CD8+ T cells activated *in vitro* confer immediate and long-term tumor protection *in vivo*. Eur J Immunol 2008;38:2886–95.
40. Imai N, Ikeda H, Tawara I, Shiku H. Tumor progression inhibits the induction of multifunctionality in adoptively transferred tumor-specific CD8+ T cells. Eur J Immunol 2009;39:241–53.
41. Kaplan DH, Shankaran V, Dighe AS, Stockert E, Aguet M, Old LJ, et al. Demonstration of an interferon gamma-dependent tumor surveillance system in immunocompetent mice. Proc Natl Acad Sci U S A 1998;95:7556–61.
42. Shankaran V, Ikeda H, Bruce AT, White JM, Swanson PE, Old LJ, et al. IFNgamma and lymphocytes prevent primary tumour development and shape tumour immunogenicity. Nature 2001;410:1107–11.
43. Koebel CM, Vermi W, Swann JB, Zerafa N, Rodig SJ, Old LJ, et al. Adaptive immunity maintains occult cancer in an equilibrium state. Nature 2007;450:903–7.
44. Schreiber RD, Old LJ, Smyth MJ. Cancer immunoediting: integrating immunity's roles in cancer suppression and promotion. Science 2011;331:1565–70.

Published OnlineFirst August 15, 2014; DOI: 10.1158/2326-6066.CIR-14-0098

AACR American Association for Cancer Research

Cancer Immunology Research

Cytotoxic T Lymphocytes Block Tumor Growth Both by Lytic Activity and IFN γ-Dependent Cell-Cycle Arrest

Hirokazu Matsushita, Akihiro Hosoi, Satoshi Ueha, et al.

Cancer Immunol Res 2015;3:26-36. Published OnlineFirst August 15, 2014.

Published OnlineFirst February 20, 2015; DOI: 10.1158/2326-6066.CIR-14-0190

Research Article

Cancer Immunology Research

Robust Antitumor Effects of Combined Anti-CD4-Depleting Antibody and Anti-PD-1/PD-L1 Immune Checkpoint Antibody Treatment in Mice

Satoshi Ueha[1], Shoji Yokochi[1,2], Yoshiro Ishiwata[1,2], Haru Ogiwara[1], Krishant Chand[1], Takuya Nakajima[1], Kosuke Hachiga[1,2], Shigeyuki Shichino[1], Yuya Terashima[1], Etsuko Toda[1], Francis H.W. Shand[3], Kazuhiro Kakimi[4], Satoru Ito[1,2], and Kouji Matsushima[1]

Abstract

Depletion of $CD4^+$ cells in tumor-bearing mice has strong antitumor effects. However, the mechanisms underlying these effects and the therapeutic benefits of $CD4^+$ cell depletion relative to other immunotherapies have not been fully evaluated. Here, we investigated the antitumor effects of an anti-CD4-depleting mAb as a monotherapy or in combination with immune checkpoint mAbs. In B16F10, Colon 26, or Lewis lung carcinoma subcutaneous tumor models, administration of the anti-CD4 mAb alone had strong antitumor effects that were superior to those elicited by $CD25^+$ Treg depletion or other immune checkpoint mAbs, and which were completely reversed by $CD8^+$ cell depletion. $CD4^+$ cell depletion led to the proliferation of tumor-specific $CD8^+$ T cells in the draining lymph node and increased infiltration of $PD\text{-}1^+CD8^+$ T cells into the tumor, with a shift toward type I immunity within the tumor. Combination treatment with the anti-CD4 mAb and immune checkpoint mAbs, particularly anti-PD-1 or anti-PD-L1 mAbs, synergistically suppressed tumor growth and greatly prolonged survival. To our knowledge, this work represents the first report of robust synergy between anti-CD4 and anti-PD-1 or anti-PD-L1 mAb therapies. *Cancer Immunol Res; 3(6); 1–10.* ©2015 AACR.

Introduction

Immune checkpoint modulators such as those targeting cytotoxic T-lymphocyte–associated antigen-4 (CTLA-4) and programmed cell death-1 (PD-1) have attracted attention due to their extraordinary antitumor effects in patients with advanced melanoma, lung cancer, and renal cancer (1, 2). An mAb against CTLA-4 (ipilimumab) that enhances both early T-cell activation and CTL function was approved for treatment of patients with advanced melanoma in the United States in 2011. An anti–PD-1 mAb (nivolumab) that protects activated T cells from exhaustion in peripheral tissues was approved for treatment of patients with melanoma in Japan and in the United States in 2014. In addition, other mAbs against CTLA-4 (tremelimumab), PD-1 (pembrolizumab), and programmed death-ligand 1 (PD-L1, a ligand for PD-1) are currently undergoing clinical trials to evaluate their antitumor efficacy. However, despite clear survival benefits in a subset of tumor patients, other groups of patients are refractory to these single-agent therapies.

Combination therapies comprising immune checkpoint modulators that have different points of action, targeting, for example, the activation and expansion of T cells in lymphoid tissues and the exhaustion and deletion of T cells in the effector site, represent promising strategies for tumor immunotherapy (1). Synergistic antitumor effects in advanced melanoma have been reported with a combination of anti–CTLA-4 and anti–PD-1 mAbs (3). The antitumor efficacy of other combinations of regulators of lymphocyte activation and expansion (e.g., Lymphocyte activation gene-3/LAG-3, OX40/CD134) and of lymphocyte exhaustion and deletion (e.g., T-cell immunoglobulin mucin-3/TIM-3, 4-1BB/CD137, B- and T-lymphocyte attenuator/BTLA, glucocorticoid-induced TNF-receptor/GITR) is currently under investigation. Because immune checkpoint modulators play both positive and negative roles in the immune inhibitory pathway with some redundancy, identification of optimal therapeutic combinations remains a considerable challenge.

Another approach to immune checkpoint modulation involves depleting immunosuppressive leukocyte populations such as forkhead box P3 $(Foxp3)^+CD25^+$ regulatory T cells (Treg), Th2 cells, T regulatory (Tr) 1/3 cells (4), myeloid-derived suppressor cells (MDSC) and indoleamine-2,3-dioxygenase $(IDO)^+$ plasmacytoid DCs (pDC; refs. 5–7). Several groups have suggested that depletion of $CD4^+$ cells, including Tregs, Th2 cells, Tr1/3 cells, and a subpopulation of MDSCs and pDCs, results in strong antitumor effects in mouse models due to the enhancement of CTL responses (8–12). These antitumor effects may be associated with the modulation of multiple immune checkpoints caused by

[1]Department of Molecular Preventive Medicine, Graduate School of Medicine, The University of Tokyo, Tokyo, Japan. [2]IDAC Theranostics, Inc., Tokyo, Japan. [3]Department of Pharmacology and Therapeutics, The University of Melbourne, Melbourne, Victoria, Australia. [4]Department of Immunotherapeutics, The University of Tokyo Hospital, Tokyo, Japan.

Note: Supplementary data for this article are available at Cancer Immunology Research Online (http://cancerimmunolres.aacrjournals.org/).

S. Ueha, S. Yokochi, and Y. Ishiwata contributed equally to this article.

Corresponding Author: Kouji Matsushima, The University of Tokyo, 7-3-1 Hongo, Bunkyo-ku, Tokyo 1130033, Japan. Phone: 81-3-5841-3431; Fax: 81-3-5684-2297; E-mail: koujim@m.u-tokyo.ac.jp

doi: 10.1158/2326-6066.CIR-14-0190

Published OnlineFirst February 20, 2015; DOI: 10.1158/2326-6066.CIR-14-0190

$CD4^+$ cell depletion. However, the relative advantage of $CD4^+$ cell depletion over other immune checkpoint mAb-based treatments remains unclear. Encouraged by the positive reports surrounding the benefits of anti-CD4 mAb treatment in mice, and by the recent clinical data supporting anti–CTLA-4 and anti–PD-1 mAb therapies, here, we examine whether treatments that combine an anti-CD4 mAb and immune checkpoint modulators produce synergistic antitumor activity.

Thus, in the present study, we used comprehensive immunologic analyses to compare the antitumor effects of an anti–CD4-depleting mAb with those of a variety of mAbs against immune checkpoint molecules, including PD-1, PD-L1, PD-L2, CTLA-4, OX40, LAG-3, TIM-3, BTLA, and GITR, in mouse subcutaneous tumor models. We also investigated the antitumor effects of treatments that combined an anti-CD4 mAb and antibodies against these immune checkpoint molecules. We report that treatment with an anti-CD4 mAb alone induces strong antitumor effects and expansion of tumor-specific $CD8^+$ T cells, and that combination of an anti-CD4 mAb with anti–PD-1 or anti–PD-L1 mAbs results in striking synergy in the suppression of tumor growth.

Materials and Methods

Mouse

Seven-week-old female C57BL/6 and male BALB/c mice were purchased from Japan SLC. Fluorescent ubiquitination-based cell-cycle indicator (Fucci) double transgenic mice were generated by crossbreeding FucciG_1-#639 and FucciS/G_2/M-#474 animals (obtained from Dr. A. Miyawaki through the RIKEN BRC) as described previously (13). Mice transgenic for the gp100 melanoma antigen-specific Pmel-1-TCR or the ovalbumin-specific OT-I TCR were purchased from The Jackson Laboratory. Each experimental group contained 8 mice except where otherwise specified. All animal experiments were conducted in accordance with institutional guidelines with the approval of the Animal Care and Use Committee of the University of Tokyo.

Cell lines and tumor models

B16F10 and Lewis lung carcinoma (LLC) were obtained from the ATCC. Colon 26 was obtained from the Cell Resource Center for Biomedical Research, Institute of Development, Aging, and Cancer, Tohoku University. B16F10 cells expressing the truncated form of human low-affinity nerve growth factor receptor (ΔhLNGFR/hCD271) were generated by retroviral transduction and two subsequent rounds of *in vivo* passaging (Supplementary Fig. S1). B16F10 cells (5×10^5/mouse), LLC cells (5×10^5/mouse), and Colon 26 cells (2×10^5/mouse) were inoculated s.c. into the right flanks of C57BL/6 or BALB/c mice. Tumor diameter was measured twice weekly and used to calculate tumor volume (mm^3) [(major axis; mm) × (minor axis; $mm)^2 \times 0.5236$].

In vivo antibody treatment

Anti-CD4 (clone GK1.5), anti-CD8 (clone YTS169.4), anti–PD-1 (clone J43), anti–PD-L1 (clone 10F.9G2), anti–PD-L2 (clone TY25), anti-OX40 (clone OX-86), anti–CTLA-4 (clone 9D9), anti–LAG-3 (clone C9B7W), anti-BTLA (clone 6A6), anti–TIM-3 (clone RMT3-23), anti-GITR (clone DTA-1), and anti-CD25 (clone PC-61.5.3) mAbs were purchased from BioXcell. Antibodies were injected i.p. at a dose of 200 μg per mouse. Anti-CD4 mAb (200 μg/mouse) was administered in a single dose or in successive doses on days 5 and 9 after tumor inoculation. Immune checkpoint antibodies (200 μg/mouse) were administered on days 4, 8, 14, and 18 after tumor inoculation. Combination treatments with the anti-CD4 mAb and anti-immune checkpoint antibodies were administered under the same conditions as respective single-agent protocols.

Immunohistologic analysis

Immunofluorescent staining was performed as described previously (14–16) using primary antibodies and the appropriate fluorophore-conjugated secondary Abs as listed in Supplementary Table S1, then photographed using an SP5 confocal microscope (Leica Microsystems).

Flow cytometry

Intravascular leukocytes were stained by i.v. injection of fluorophore-conjugated mAb (3 μg/mouse) against CD45 or CD45.2 3 minutes before collecting tissues. Single-cell suspensions were prepared by enzymatic or mechanical dissociation of tissues with or without subsequent density separation, as described previously (17, 18). Flow-Count fluorospheres (Beckman Coulter) were used to determine cell numbers and normalize cell concentrations before antibody staining. Cells were pretreated with Fc Block (anti-mouse CD16/CD32 mAb; clone 2.4G2, BioXcell), then stained with mix of fluorophore-conjugated anti-mouse mAbs as indicated in Supplementary Table S1. Data were acquired on a Gallios flow cytometer (Beckman Coulter) and analyzed using FlowJo software (version 9.7.5; FlowJo, LLC). Nonviable cells were excluded from the analysis based on forward and side scatter profiles and propidium iodide staining.

Quantitative reverse transcription real-time PCR

Total RNA was extracted using a RNeasy Mini kit (Qiagen) and converted to cDNA using ReverTra Ace qPCR RT Master Mix with gDNA Remover (Toyobo) according to the manufacturer's instructions. Real-time quantitative PCR analysis was performed using THUNDERBIRD Probe qPCR Mix or THUNDERBIRD SYBR qPCR Mix (Toyobo), and an ABI 7500 sequence detector system (Life Technologies). The primers used for the PCR reaction are listed in Supplementary Table S2. The expression levels of each gene were normalized to *Rps3* expression level for each sample.

Statistical analysis

Unless otherwise stated, data are presented as mean ± SE. Statistical analyses were performed using GraphPad Prism software (version 6.0e; GraphPad Software). For comparisons between groups in the *in vivo* study, we used one-way ANOVA with the Dunnett *post hoc* test. For comparisons between the means of two variables, we used paired Student *t* tests. Comparisons of survival data between groups were made using the log-rank test after Kaplan–Meier analysis. A P value of <0.05 was considered to be statistically significant.

Results

An optimized anti-CD4 mAb treatment protocol exerts robust antitumor effects

We began by optimizing the protocol for anti-CD4 mAb administration in B16F10, LLC and Colon 26 tumor models. Mice bearing subcutaneous tumors received a single i.p. injection of 200 μg anti-CD4 mAb 2 days before (day −2) or 0, 3, 5, or

Published OnlineFirst February 20, 2015; DOI: 10.1158/2326-6066.CIR-14-0190

9 days after tumor inoculation. In all three models, administration of anti-CD4 mAb on days 3 and 5 significantly suppressed tumor growth (Supplementary Fig. S2A–S2C). B16F10 tumor growth, but not LLC and Colon 26 tumor growth, was also inhibited by mAb administration on days −2 and 0 (Supplementary Fig. S2A). However, the growth of LLC and Colon 26 tumors was not significantly affected by mAb administration at days −2 and 0 (Supplementary Fig. S2B and S2C). Successive administration of the anti-CD4 mAb on days 5 and 9 resulted in the greatest inhibition of tumor growth in all three models (data not shown). Doses of anti-CD4 mAb (3.1 or 12.5 μg/mouse) that were insufficient to cause CD4 lymphocyte depletion had no inhibitory effect on tumor growth in the melanoma model (Supplementary Fig. S2D and S2E). On the basis of these results, for subsequent studies, we adopted a protocol of administering the anti-CD4 mAb at a dose of 200 μg/mouse successively on days 5 and 9 after tumor inoculation.

We next compared the antitumor effects of the anti-CD4 mAb against those of a variety of immune checkpoint mAbs (PD-1, PD-L1, PD-L2, CTLA-4, OX40, LAG-3, TIM-3, BTLA, and GITR) in the B16F10 model, because melanoma is a major target of anti-immune checkpoint antibody therapy. We found that twice-weekly injections of immune checkpoint antibodies were sufficient to produce the same level of antitumor effect as achieved with daily injections (data not shown). Among the mAbs tested, the anti-CD4 mAb was the most effective single-agent treatment in terms of tumor growth inhibition and survival (Fig. 1A–C). Collectively, these results confirm the potent antitumor effects of anti-CD4 mAb treatment in mice and reveal a surprising advantage of anti-CD4 mAb treatment over immune checkpoint mAb treatment.

Anti-CD4 mAb treatment depletes $CD4^+$ T cells and pDCs

To determine which cells are depleted by anti-CD4 mAb therapy, we next examined changes in cell populations with immunosuppressive potential following anti-CD4 mAb administration at day 5 in mice bearing B16F10 tumors. Flow cytometric analysis revealed that numbers of $CD4^+$ T cells, including $Foxp3^+$ $CD25^+$ Tregs, decreased 50- to 100-fold over days 2 to 9 following anti-CD4 mAb administration (7 to 14 days after tumor inoculation), as compared with cell numbers in phase-matched untreated tumor-bearing mice (Supplementary Fig. S3A–S3C). When LLC tumor-bearing mice were administered anti-CD4 mAb on days 5 and 9, $CD4^+$ T cells disappeared from the blood until at least day 15 after the first mAb administration (Supplementary Fig. S3D). pDCs, a subset of which are positive for CD4 and have been implicated in the suppression of antitumor immune responses (7), also decreased 3- to 10-fold over days 2 to 9 following mAb treatment (Supplementary Fig. S3A–S3C). MDSC subpopulations, including neutrophils and Ly-$6C^{hi}$ or Ly-$6C^{lo}$ monocytes, were not significantly affected by mAb treatment (data not shown). These results indicate that $CD4^+$ T cells (including Tregs) and pDCs are the targets of anti-CD4 mAb therapy.

Anti-CD4 mAb treatment increases the number of tumor-infiltrating $CD8^+$ T cells

We next investigated the effects of anti-CD4 mAb therapy on tumor-infiltrating $CD8^+$ T-cell populations. Intravascular staining (IVS) is a technique that allows circulating leukocytes present in tissue blood vessels (which represent a proportion of total leukocytes recovered) to be distinguished from cells

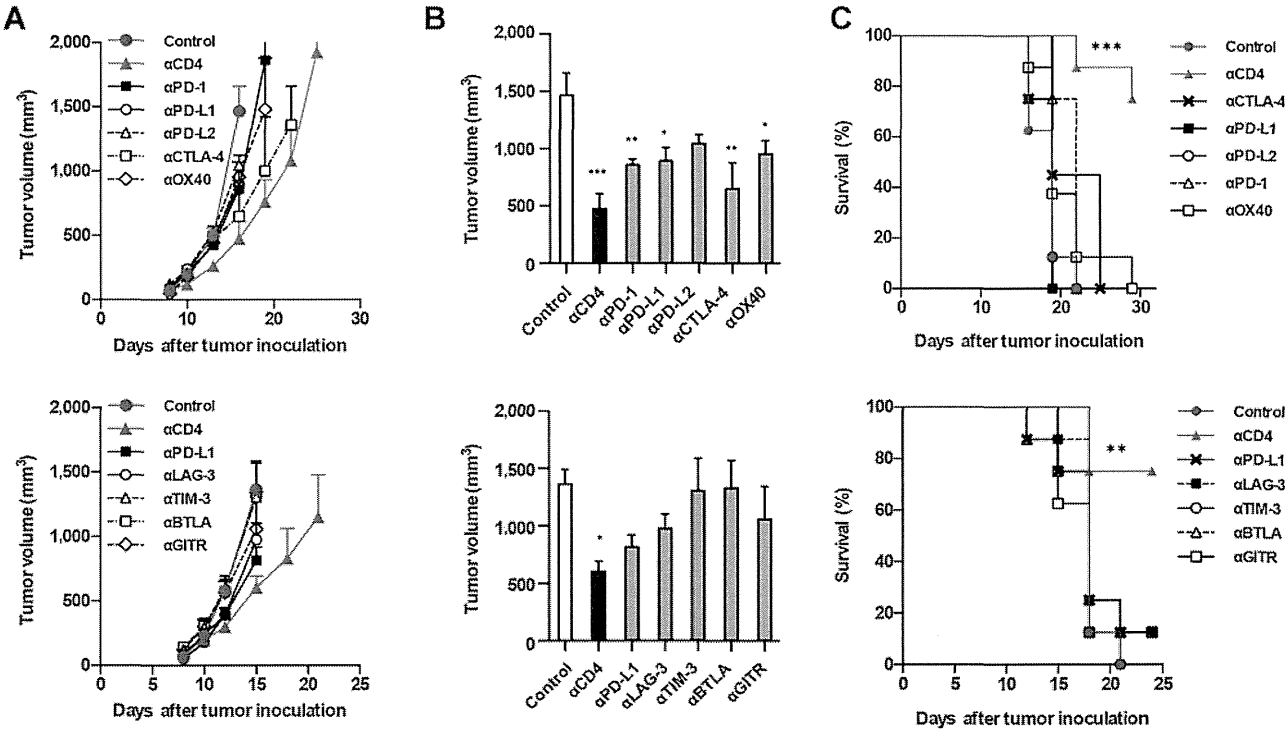

Figure 1.

Antitumor effects of anti-CD4 mAb treatment. Mice bearing B16F10 melanoma tumors were injected i.p. with anti-CD4 mAb (200 μg/mouse) on days 5 and 9 or anti-immune checkpoint mAbs on days 4, 8, 14, and 18 after tumor inoculation. A, tumor growth curves. B, tumor volume on day 16 (top) or day 15 (bottom). C, survival following tumor inoculation (8 mice/group). A and B, data, mean ± SE of 8 mice per group; *, $P < 0.05$; **, $P < 0.01$; ***, $P < 0.001$ (compared with control).

Published OnlineFirst February 20, 2015; DOI: 10.1158/2326-6066.CIR-14-0190

actually infiltrating the parenchyma of tissues, including tumors (19). In untreated B16F10 tumors, about 15% of $CD8^+$ T cells were positive for IVS, and the frequency of $PD\text{-}1^+CD137^+$ tumor-reactive cells (20) was about 10-fold lower in this population than in the IVS-negative parenchymal cell population (Supplementary Fig. S4A and S4B). Anti-CD4 mAb treatment significantly increased the frequency and number of IVS-$CD45^-CD8^+$ T cells in the tumor (Fig. 2A and B). The increased number of $CD8^+$ T cells in the tumors of anti-CD4 mAb-treated mice was also evident in histologic sections (Fig. 2C). Furthermore, the IVS$^-CD8^+$ T cells induced by anti-CD4 mAb treatment contained a higher proportion of $PD\text{-}1^+CD137^+$ tumor-reactive cells (Fig. 2D and E), had greater potential to produce IFNγ in response to *ex vivo* PMA/ionomycin stimulation (Fig. 2F and G), and showed higher specific killing activity against B16F10 tumor cells (Supplementary Fig. S5A–S5C), compared with T cells from the untreated group. In the LLC and Colon 26 tumor models, anti-CD4 mAb-treated mice displayed decreased tumor growth, systemically increased $CD8^+CD44^{hi}PD\text{-}1^+$ T cells, and upregulation of LAG-3, TIM-3, and CTLA-4 in tumor-infiltrating $CD8^+$ T cells (Supplementary Fig. S6A–S6D). Collectively, these results suggest that anti-CD4 mAb treatment enhances antitumor $CD8^+$ T-cell responses and induces a shift toward type I immunity within the tumor.

Anti-CD4 mAb treatment promotes expansion of tumor-specific $CD8^+$ T cells in the draining lymph node

To further investigate the effects of anti-CD4 mAb treatment on tumor-specific $CD8^+$ T-cell responses, we adoptively transferred melanoma antigen-specific Pmel-1 TCR transgenic $CD8^+$ T cells (21) into mice 1 day before inoculation with B16F10 tumors (day −1; Supplementary Fig. S7A and S7B). On day 14 after tumor inoculation, numbers of Pmel-1 $CD8^+$ T cells in the blood, draining lymph node (dLN), non-dLN (ndLN), spleen and tumor were 10- to 100-fold higher in anti-CD4 mAb-treated mice compared with that in untreated mice (Supplementary Fig. S7C and S7D). As tumors grew, Pmel-1 $CD8^+$ T-cell numbers were unchanged or decreased in untreated group mice, whereas Pmel-1 $CD8^+$ T-cell numbers increased in anti-CD4 mAb-treated mice (Supplementary Fig. S7E). To determine the site of Pmel-1 $CD8^+$ T-cell expansion, we administered bromodeoxyuridine (BrdUrd) 1 hour before collecting tissues. The number of $BrdU^+$-proliferating Pmel-1 $CD8^+$ T cells in the dLN far outnumbered those in the tumor, irrespective of anti-CD4 mAb treatment (Supplementary Fig. S7F and S7G). Importantly, proliferating cell numbers decreased between days 9 and 14 in untreated mice, but increased in anti-CD4 mAb-treated mice (Supplementary Fig. S7H). Similar CD4 depletion–induced proliferation was also observed in endogenous polyclonal $CD8^+$ T cells (data not shown). These data suggest that anti-CD4 mAb treatment protects tumor-reactive

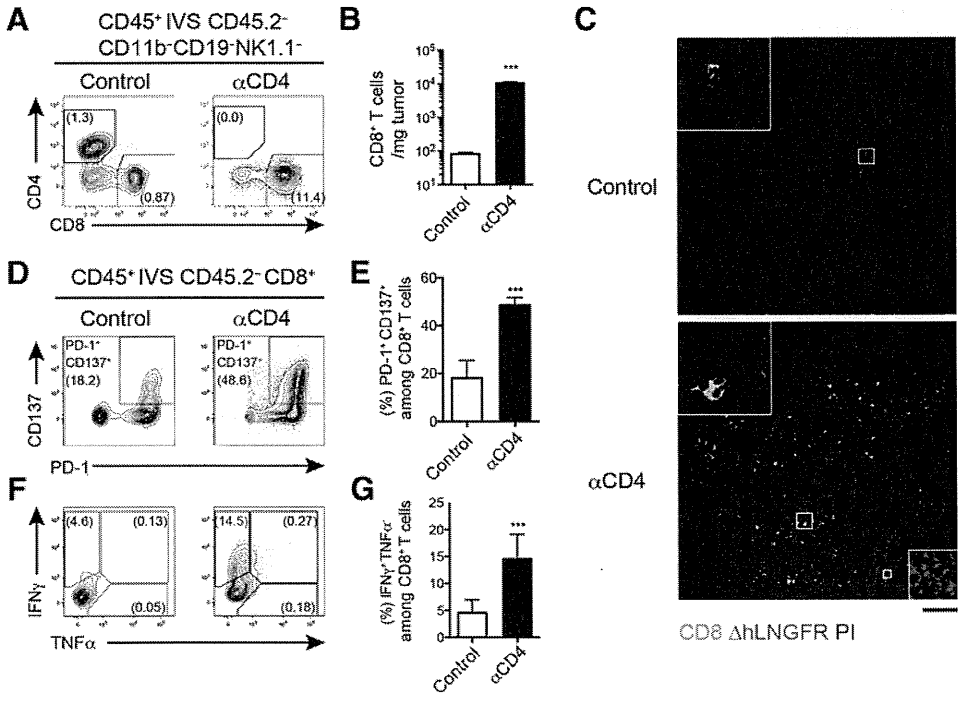

Figure 2.
Anti-CD4 mAb treatment increases the number of tumor-infiltrating $CD8^+$ T cells. Mice bearing B16F10 (A, B, D–G) or B16F10-ΔhLNGFR (C) tumors were injected i.p. with anti-CD4 mAb on days 5 and 9, and tumor-infiltrating $CD8^+$ T cells were analyzed on day 14 after tumor inoculation. Control mice received an injection of vehicle only. For flow cytometric analyses, mice were given an i.v. injection of anti-CD45.2 Ab 3 minutes before the collection of tissues to enable identification of cells in the blood compartment (IVS). A, flow-cytometry plots of parenchymal leukocyte compartments ($CD45^+$IVS-$CD45.2^-$). B, the number of parenchymal $CD8^+$ T cells in tumor. C, distribution of $CD8^+$ T cells in the tumor. Green, CD8; red, ΔhLNGFR; blue, propidium iodide (PI). Enlargements in white boxes show nonnecrotic areas, yellow box shows necrotic area; scale bar, 200 μm. D, flow-cytometry plots and frequencies (E) of $PD\text{-}1^+CD137^+$ tumor-reactive cells among the parenchymal $CD8^+$ T-cell population. F, flow-cytometry plots and frequencies (G) of IFNγ- and TNFα-producing cells among the parenchymal $CD8^+$ T-cell population following *ex vivo* restimulation with PMA and ionomycin. Data represent mean ± SE of 4 mice per group and are representative of at least four independent experiments. Numbers in flow-cytometry plots indicate mean frequencies within live cells (A) or parental populations (D and F); ***, $P < 0.001$ (compared with control).